KDM2B promotes cell viability by enhancing DNA damage response in canine hemangiosarcoma

Kevin Christian Montecillo Gulay [a], Keisuke Aoshima [a, *], Yuki Shibata [b], Hironobu Yasui [b], Qin Yan[c], Atsushi Kobayashi [a] & Takashi Kimura [a]

[a] Laboratory of Comparative Pathology, Department of Clinical Sciences, Faculty of Veterinary Medicine, Hokkaido University, Sapporo, Hokkaido, 060-0818, Japan.

[b] Laboratory of Radiation Biology, Department of Applied Veterinary Sciences, Faculty of Veterinary Medicine, Hokkaido University, Sapporo, Hokkaido, 060-0818, Japan.

[c] Department of Pathology, Yale School of Medicine, New Haven, CT, USA.

* Corresponding author

E-mail address: k-aoshima@vetmed.hokudai.ac.jp

Competing interests

19 The authors declare no competing interests.

20

Abstract

Epigenetic regulators have been implicated in tumorigenesis of many types of cancer; however, their roles in endothelial cell cancers such as canine hemangiosarcoma (HSA) have not been studied. In this study, we find that lysine-specific demethylase 2b (KDM2B) is highly expressed in HSA cell lines compared to normal canine endothelial cells. Silencing of KDM2B in HSA cells results in increased cell death *in vitro* compared to the scramble control by inducing apoptosis through the inactivation of the DNA repair pathways and accumulation of DNA damage. Similarly, doxycycline-induced KDM2B silencing in tumor xenografts results in decreased tumor sizes compared to the control. Furthermore, KDM2B is also highly expressed in clinical cases of HSA. We hypothesize that pharmacological KDM2B inhibition can also induce HSA cell death and can be used as an alternative treatment for HSA. We treat HSA cells with GSK-J4, a histone demethylase inhibitor, and find that GSK-J4 treatment also induces apoptosis and cell death. In addition, GSK-J4 treatment decreases tumor sizes. Therefore, we demonstrate that KDM2B acts as an oncogene in HSA by enhancing the DNA damage response. Moreover, we show that histone demethylase inhibitor GSK-J4 can be used as a therapeutic alternative to doxorubicin for HSA treatment.

Keywords

DNA repair, epigenetics, hemangiosarcoma, KDM2B, oncogene

1. Introduction

Canine hemangiosarcoma (HSA) is a highly malignant tumor of vascular endothelial cells. It is an aggressive tumor with high rates of local recurrence and metastasis, and a low

43 overall survival time (Kim et al., 2015). Its high cellular heterogeneity has limited genomic and
44 pathogenesis studies in HSA. Genomic analyses have revealed that HSA cells have somatic
45 coding mutations in the *TP53*, *PIK3CA*, and *PIK3R1*. Furthermore, *CDKN2A/B* were found to
46 be consistently deleted and copies of *VEGFA*, *KDR* and *KIT* were gained (Megquier et al., 2019).
47 The oncogene involved in HSA, however, is still unknown.

48 Epigenetic mechanisms are essential for reproduction, embryonic development, and
49 maintenance of normal cell function in eukaryotes (Sharma et al., 2009). Generally, the genetic
50 alterations that cause tumorigenesis are combined with epigenetic shifts, such as aberrant DNA
51 methylation and histone modifications, which may help oncogenic drivers improve cancer
52 development, metastasis, and resistance to therapies (Moosavi and Ardekani, 2016). KDM2B
53 (also known as NDY1 and FBXL10), an H3K4me3, H3K36me2/3 and H3K79me3 demethylase,
54 acts as a tumor suppressor in gastric cancer by downregulating glycolysis, and tumor-derived
55 mutation in KDM2B enhances cell proliferation through the inability of c-FOS degradation
56 (Hong et al., 2016). Alternatively, KDM2B can also act as an oncogene in various types of
57 cancers. In leukemia, KDM2B is highly expressed and is sufficient to transform hematopoietic
58 progenitor cells (He et al., 2011). In breast cancer, KDM2B regulates Polycomb repressive
59 complexes and controls the self-renewal of breast cancer stem cells (Kottakis et al., 2014). This
60 bifunctional activity means that the role of KDM2B in tumors is highly context dependent and

must be evaluated carefully (Yan et al., 2018). While epigenetics is highly involved in the pathogenesis of many cancers, its role in HSA is still unknown.

Treatment of HSA is carried out by tumor excision and chemotherapy mainly with doxorubicin (Clifford et al., 2000). The mean survival time for surgical treatment is three months while the mean survival time for surgical treatment with chemotherapy is less than a year (Batschinski et al., 2018). Chemotherapeutic drugs fail to improve survival times of cancer patients due to the non-specificity of their cytotoxic effects in the cardiomyocytes, brain, liver and intestine (Odom et al., 1992; Carvalho et al., 2009). A more effective, specific, and safer treatment for HSA is warranted.

Histone demethylase inhibitors are effective agents for anticancer treatment. In a previous study, GSK-J4, a histone demethylase inhibitor, decreased AML disease progression by downregulating DNA replication and cell cycle-related pathways through the enrichment of H3K27me3 (Li et al., 2018). GSK-J4 was initially developed as a KDM6 inhibitor, but it was found to inhibit the catalytic activity of a wide range of JmjC domain-containing histone demethylases including KDM2B (Heinemann et al., 2014). Epigenetic therapy may provide additional treatment options, but no epigenetic drug has been tested in HSA.

In this study, we sought to study the role of epigenetic regulators in HSA to improve our understanding of the etiology and pathogenesis of HSA and to find an alternative for

doxorubicin treatment in HSA.

2. Results

2.1. KDM2B is important for HSA cell survival

We first performed RNA-sequencing analysis of canine aortic endothelial cells (CnAOEC) and one HSA cell line, JuB2, to examine the expression levels of epigenetic modifiers. Among the differentially expressed genes, histone methyltransferases/demethylases, histone acetyltransferases/deacetylases, and DNA methyltransferase/demethylases were dysregulated in JuB2 compared with CnAOEC (Figs. 1A and S1A). Next, we performed qRT-PCR to verify RNA-seq results of histone methyltransferases/demethylases in CnAOEC and seven HSA cell lines. The result indicated that some histone methyltransferases/demethylases were highly upregulated in HSA cell lines at gene expression levels (Figs. 1B and S1B). While histone demethylases were relatively stable between HSA cells and CnAOEC compared with histone methyltransferase, three histone demethylases (*KDM1A, KDM2A* and *KDM2B*) were markedly upregulated. We performed western blotting for KDM1A, KDM2A, and KDM2B and found that their protein levels were upregulated in all HSA cell lines compared with CnAOEC (Fig. 1C and 1D). These results suggest that epigenetic regulators are dysregulated in HSA and that histone demethylases KDM1A, KDM2A, and

KDM2B are highly expressed in HSA.

To examine whether the overexpression of KDM1A, KDM2A and KDM2B have important functional roles in HSA, we designed three shRNA sequences for each gene to knockdown *KDM1A*, *KDM2A* and *KDM2B*. We also designed two scramble shRNAs (scrRNA) to serve as controls. These shRNAs were expressed in HSA cell lines using a doxycycline (Dox)-inducible vector system. Knockdown was verified with western blotting after four days of Dox treatment (Figs. 2A and S2A)**.** Knockdown of *KDM1A* and *KDM2A* did not have short-term effects on JuB2 cell viability, whereas knockdown of *KDM2B* significantly decreased JuB2 cell viability within four days (Figs. 2B and S2B). To evaluate the long term effects of KDM1A, KDM2A, and KDM2B silencing on JuB2 cell survival, we performed colony formation assay and found that *KDM1A* or *KDM2A* knockdown inhibited JuB2 colony formation,, whereas *KDM2B* knockdown significantly reduced the number of colonies of JuB2 (Figs. 2C, 2D, S2C, S2D). KDM2B knockdown with constitutively expressed shRNA vectors also induced the same phenotype in JuB2 cells and other HSA cell lines such as JuB4, Re21, and Ud6 (Fig. S3A and S3B). These results suggest that KDM2B is an important histone demethylase in HSA cell survival. To examine whether KDM2B can alter global histone methylation and ubiquitination levels in HSA cell lines, we performed western blotting for histone methylations and ubiquitination which can be modified by KDM2B itself or complexes

115 containing KDM2B. We found that H2AK119ub1 levels were globally decreased in KDM2B
116 knockdown cells while other histone modifications were not affected (Fig. 2E). Next, to
117 investigate which KDM2B domain is responsible for HSA cell viability, we rescued KDM2B
118 function in *KDM2B* silenced HSA cells. We expressed wild type (WT) canine KDM2B with
119 silent mutations for the sequences which were targeted by the shRNAs, and KDM2B mutants
120 with a point mutation for the JmjC domain ($KDM2B^{H283Y}$), the CXXC domain ($KDM2B^{C586A}$),
121 or with PHD-finger domain deleted ($KDM2B^{\Delta PHD}$) (Tzatsos et al., 2009; Wang et al., 2011).
122 Overexpression of WT KDM2B and $KDM2B^{C586A}$ mutant but not the $KDM2B^{H283Y}$ nor the
123 $KDM2B^{\Delta PHD}$ mutants rescued the phenotype (Fig. 2F), which suggests that the JmjC and the
124 PHD-finger domains are important for the KDM2B function in HSA.

125 To verify our *in vitro* results and to know the effect of *KDM2B* silencing *in vivo*, JuB2
126 cells with Dox-inducible shRNAs for *KDM2B* or the scramble shRNA were injected
127 subcutaneously into nude mice and the tumor volumes over time were measured.
128 Dox-containing food pellets were provided to the mice to induce shRNA expression when the
129 largest tumor reached 150 mm^3 in volume. Tumor xenografts started to decrease in volume four
130 days after induction of KDM2B silencing, moreover, half of the xenografts bearing
131 shKDM2B-A and one out of eight xenografts bearing shKDM2B-C completely regressed ten
132 days post-induction (Fig. 2G and 2H). At the endpoint, tumor xenografts with silenced KDM2B

had significantly decreased tumor weights compared with the xenografts overexpressing the scramble shRNA control (Fig. 2I). We also xenografted JuB2 cells expressing the silencing vector for KDM1A or KDM2A. Although tumor volume repression was initially observed post-doxycycline treatment, tumor regrowth was observed ten days post-doxycycline treatment signifying that other histone demethylases or proteins can rescue KDM1A or KDM2A function *in vivo* or some cell populations were not affected by their knockdown (Fig. 2G).

These results suggest that KDM2B is important for HSA cell survival both *in vitro* and *in vivo* and its local catalytic activity is responsible for the phenotype.

2.2. KDM2B knockdown induces apoptosis via accumulation of DNA damages

To understand the mechanisms by which KDM2B regulates HSA cell survival, we performed RNA-seq followed by gene set enrichment analysis (GSEA) in JuB2 cells expressing shKDM2B-A versus JuB2 cells expressing scrRNA-1. Silencing of *KDM2B* showed negative correlations with angiogenesis and glycolysis pathways, which might reflect decreased HSA cell viability (Fig. S4A). Interestingly, expressions of genes downregulated in response to ultraviolet (UV) radiation (HALLMARK_UV_RESPONSE_DN) were decreased by *KDM2B* knockdown (Fig. 3A). Considering this correlation and the fact that UV response can trigger DNA damage response (Stokes et al., 2007), we speculated that DNA damage might be related to *KDM2B*

151 knockdown phenotypes. This speculation was further supported by positive enrichment of the
152 G2M checkpoint and the interferon response pathways, which have been reported to be
153 associated with mitochondrial and nuclear DNA damages (Fig. S4A) (Brzostek-Racine et al.,
154 2011; Mboko et al., 2012; Chen et al., 2020). These results were validated by qRT-PCR (Figs.
155 3B, S4B, S4C, S4D, S4E). Next, we performed Cleavage Under Target & Release Using
156 Nuclease (CUT&RUN) to examine whether H2AK119ub1 and H3K4me3 levels at the
157 promoters or gene bodies of *GAPDH, KDM2B,* and KDM2B target genes (*INSIG1* and *OAS2*)
158 were affected by *KDM2B* knockdown. Consistent with global decrease in H2AK119ub1 by
159 *KDM2B* knockdown, we found that H2AK119ub1 at the promoter regions of *GAPDH* and
160 *OAS2* were significantly decreased in *KDM2B* knockdown cells while H2AK119ub1 at the gene
161 bodies were not affected (Fig. 3C). H3K4me3 levels at the promoter regions were decreased in
162 *GAPDH* and *INSIG1* and increased in *OAS2* in *KDM2B* knockdown cells, which was consistent
163 with their gene expression changes (Figs. 3B, 3C, S4B). To further dissect the mechanism, we
164 examined the expression levels of proteins involved in DNA repair pathway. Total ATM, c-FOS,
165 and γH2A.X expressions were upregulated in HSA cell lines compared to CnAOEC and their
166 expressions were significantly decreased by *KDM2B* knockdown (Fig. 3D and 3E).
167 Phosphorylated-ATM (pATM), an active form of ATM, was also decreased by *KDM2B*
168 knockdown. Next, we carried out alkaline comet assay to detect DNA strand breaks in HSA cell

lines upon *KDM2B* silencing. Our results showed that *KDM2B* silencing drastically increased tail DNA percentages, tail lengths, and tail momentums compared to the scramble control (Fig. 3F and 3G). Furthermore, flow cytometry analysis using propidium iodide (PI) revealed that JuB2 with silenced *KDM2B* increased aneuploid peaks although parental HSA cells also showed aneuploidy (Figs 4A, 4B, S5A, S5B). In contrast, overexpression of WT KDM2B in JuB2 HSA cells resulted to significantly decreased aneuploid cell population compared to empty vector (EV) expressing JuB2 cells (Fig. 4C and 4D). In addition, active apoptosis markers, cleaved-caspase 3, BAX, and phosphorylated ERK1/2 (pERK1/2), were increased in cells with silenced *KDM2B* compared to the scramble control cells (Fig. 4E). Furthermore, overexpression of KDM2B in CnAOEC decreased the pERK1/2 expression compared to the EV control (Fig. 4F and 4G) and repressed mRNA expressions of cell cycle checkpoint genes such as $p15^{ink4b}$, $p16^{ink4a}$, and *ATR* (Fig. 4H). These results suggest that *KDM2B* knockdown in HSA cells induces cell death via apoptosis caused by the accumulation of DNA damages due to the low expression of proteins involved in DNA repair.

2.3. KDM2B is highly expressed in clinical cases of HSA

We demonstrated that KDM2B upregulation was important for HSA cell survival, but KDM2B expression in clinical HSA cases has not been investigated. To this end, we analyzed

187 seventeen clinical cases of HSA and compared the immunohistochemical KDM2B expression
188 between HSA cells and normal endothelial cells in the same sample. Our results showed that
189 KDM2B was highly expressed in HSA cells compared to normal endothelial cells in almost all
190 the cases examined regardless of proliferation patterns or degree of differentiation (Fig. 5A and
191 5B). The average KDM2B score in HSA cells was significantly higher than that in normal
192 endothelial cells (Fig. 5C). We then also examined the benign endothelial tumor, hemangioma
193 (HMA), for KDM2B expression. Interestingly, KDM2B expression levels in hemangioma cells
194 were likely lower than normal endothelial cells in the same sample (P = 0.096; Fig. 5D–5F,).
195 The average KDM2B expression scores in HSA were significantly higher than in HMA cells
196 when the average KDM2B scores in tumor cells were normalized to normal endothelial cells in
197 the same slides (Fig. 5G). KDM2B expressions were also analyzed in histologically-similar
198 tumors, hemangiopericytoma (HPC), melanoma, and fibrosarcoma cells. Results showed that
199 HPC, melanoma, and fibrosarcoma cells had similar KDM2B expression compared to normal
200 endothelial cells in the same slide (Fig. S6A–S6C). These results suggest that KDM2B
201 expresses in clinical HSA samples and can be used as a biomarker to differentiate HSA and
202 HMA. In addition, KDM2B may also be used as a molecular marker to differentiate HSA from
203 HPC, melanoma, and fibrosarcoma.
204

205 *2.4. GSK-J4 inhibits HSA cell viability*

206 We demonstrated that KDM2B inhibition through shRNA could induce HSA cell death.
207 Based on this, we hypothesized that pharmacological KDM2B inhibition could also induce HSA
208 cell death. To test this hypothesis, we used a histone demethylase inhibitor GSK-J4 since there
209 is no KDM2Bspecific KDM2B inhibitor available. We treated HSA cell lines with different
210 concentrations of GSK-J4 and compared it to doxorubicin-treated cells. GSK-J4 inhibited HSA
211 cell viability at a lower concentration in JuB2, JuB4, and Ud6 cell lines compared to
212 doxorubicin (Fig. 6A). HSA cell lines treated with GSK-J4 have higher expressions of
213 cleaved-caspase 3 compared to HSA cells treated with doxorubicin. In contrast, GSK-J4-treated
214 HSA cells have decreased t-ATM and γH2A.X expression compared to DMSO control-treated
215 HSA cells (Fig.6B). Global H3K4me3 level was increased four days after GSK-J4 treatment
216 while H3K79me3, H3K36me2/3, and H3K27me3 were not globally changed (Fig. S7A).

217 To determine whether GSK-J4 can be used as an alternative drug for HSA treatment,
218 we treated nude mice harboring JuB2 tumors with DMSO, GSK-J4 or doxorubicin. GSK-J4
219 treatment significantly decreased the tumor growth over time and tumor weights at the endpoint
220 compared to DMSO treatment (Fig. 6C–6E). Although Doxorubicin treatment also led to
221 decreased tumor growth, it had significant toxicity and led to 83% mortality in 21 days (Fig. 6F).
222 In contrast, GSK-J4 did not induce any death during the treatment period. Body and liver

223 weights decreased in doxorubicin-treated mice compared to DMSO or GSK-J4 treated mice
224 (Figs. 6G and S7B). In addition, increased hematopoiesis in bone marrow, a sign of
225 myelosuppression, and dilation of intestines were only observed in mice treated with
226 doxorubicin (Fig. S7C and S7D). These results suggest that GSK-J4 can selectively inhibit HSA
227 cell growth by inducing HSA cell apoptosis without any obvious side-effects. Thus, GSK-J4
228 could be used as a therapeutic alternative to doxorubicin for HSA treatment.
229
230 **3. Discussion**
231 To our knowledge this is the first study which evaluated the role of epigenetic
232 regulators in HSA. We demonstrated that KDM2B upregulation in HSA cell lines and clinical
233 samples is important for HSA cell survival by regulating DNA damage repair and apoptosis.
234 There are three possible reasons for the high expression of KDM2B in HSA. Firstly, *KDM2B*
235 upstream regulators may be dysregulated. In bladder cancer, the upregulation of fibroblast
236 growth factor-2 upregulated the KDM2B/EZH2-miR-101 pathway and promoted tumor cell
237 proliferation, survival, and migration (Kottakis et al., 2011). In squamous cell and cervical
238 carcinomas, increased copy number of *MYC* resulted to increased KDM2B expression (Peta et
239 al., 2018). Secondly, the *KDM2B* gene itself may have acquired increased copy numbers. We
240 demonstrated that parental HSA cell lines contain an aneuploid cell population. Since cell

241 aneuploidy can cause genomic instability as a result of decreased DNA damage repair activity
242 (Sheltzer et al., 2011), some genes including *KDM2B* in HSA might have increased copy
243 numbers. Lastly, *KDM2B* might be upregulated to compensate for DNA damage and to integrate
244 genetic stability in HSA genomes. As we mentioned above, flow cytometry analysis revealed
245 multiple aneuploid peaks in HSA cell lines. Aneuploidy has also been reported in clinical cases
246 of HSA and in HSA cell lines, which implies that HSA cells are subject to high level cellular
247 stress (Fosmire et al., 2004; Thomas et al., 2014; Zhu et al., 2018). In such conditions, HSA
248 cells may bypass cell death caused by accumulated cellular stresses through modulation of gene
249 expression. We showed that knockdown of KDM2B in HSA cell lines decreased DNA repair
250 protein expressions and increased DNA damage. In contrast, exogenous expression of KDM2B
251 in JuB2 and in CnAOEC increased euploid population and inhibited apoptosis, respectively.
252 KDM2B may ease cellular stress caused by DNA damage in endothelial cells by regulating the
253 DNA repair system.

254 *KDM2B* knockdown decreased global H2AK119ub1 levels (Fig. 2E) and
255 H2AK119ub1 was enriched at the promoter regions of *GAPDH* and *OAS2* (Fig. 3C).
256 H2AK119ub1 at the promoter regions is established by non-canonical PRC1.1 (van den Boom
257 et al., 2016). KDM2B is the DNA-binding subunit of non-canonical PRC1.1, which does not
258 work with PRC2 complex which catalyzes H3K27 methylation (van den Boom et al., 2016).

259 Since H2AK119ub1 was enriched at the promoter regions of *GAPDH* and *OAS2*, and *KDM2B*
260 knockdown did not change H3K27me3 levels in HSA cells, non-canonical PRC1.1 might be
261 important for HSA cell survival.

262 KDM2B and other histone demethylases are known to have a double-edged function
263 in cancer (Yan et al., 2018). A study showed that KDM2B suppresses tumorigenesis in gastric
264 cancer by enhancing c-FOS degradation, and that impairment of KDM2B through
265 patient-derived mutations enhances tumor cell proliferation (Han et al., 2016). In contrast,
266 degradation of c-FOS by KDM2B in glioblastoma multiforme can increase cancer cell
267 resistance to chemotherapy (Kurt et al., 2017). In HSA, we showed that positive regulation of
268 DNA repair genes by KDM2B can enhance HSA cellular viability in contrast to a previous
269 report where KDM2B was shown to promote colon cancer cell survival by negatively regulating
270 DNA damage response-related genes such as ATM and ATR (Chen et al., 2014). These
271 contrasting evidences support the role of KDM2B in DNA damage response and suggest that
272 the role of KDM2B in DNA damage response in cancer cells is highly context dependent.

273 We have presented various evidences which demonstrate the role of KDM2B as an
274 oncogene in HSA by regulating DNA repair system and apoptosis, and that KDM2B can be
275 used as a biomarker to aid HSA diagnosis. We also demonstrated that a histone demethylase
276 inhibitor GSK-J4 can work as a new therapeutic alternative to doxorubicin treatment in HSA.

These findings shed light on epigenetic pathology and provide a new insight for novel therapies in HSA.

4. Materials and Methods

4.1. Cell culture

The HSA cell lines were donated by Dr. Sakai (Gifu University) (Murai et al., 2012) and cultured as described previously (Aoshima et al., 2018). CnAOEC was purchased from Cell Applications (CA, USA). CnAOEC was cultured in Endothelial Cell Growth Medium 2 Kit (Takara Bio, Inc. Kusatsu, Japan). All cells used were routinely tested for *Mycoplasma* using PCR and were submitted to ICLAS Monitoring Center (Kawasaki, Japan) for Mouse hepatitis virus testing (Harasawa et al., 1993, 2005).

4.2. Mice

All mouse experiments were performed under the AAALAC guidelines in Yale University (protocol number: 2018-11286) and Hokkaido University (protocol number:19-0130). Seven-week-old female Balb/c Nude mice purchased from Charles River Laboratories (MA, USA) were used for *KDM2B* knockdown experiments. Six-week-old KSN/Slc mice purchased from Japan SLC, Inc. (Shizuoka, Japan) were used for drug treatment experiments. Mice were

295 kept in a temperature-controlled specific-pathogen-free facility on a 12 hr light/dark cycle.
296 Animals in all experimental groups were examined at least twice weekly for tumorigenesis.
297
298 *4.3. Tumor xenograft studies*
299 A day before tumor inoculation, KSN/Slc mice were treated with 100 μL of 2.5
300 mg/mL anti-asialo GM1 (Fujifilm Wako Pure Chemical Industries, Osaka, Japan) to increase the
301 success rate of transplantation by depleting NK cells (Yoshino et al., 2000). JuB2 parental HSA
302 cells and JuB2 cells expressing the shRNAs or the scramble shRNA for *KDM2B* in the presence
303 of doxycycline were cultured in 15 cm dishes without doxycycline. Mice were randomly
304 assigned to each group. Three million HSA cells were resuspended in Corning® Matrigel®
305 Basement Membrane Matrix (Corning Inc. NY, USA) and inoculated subcutaneously in mice
306 anesthetized with 3% isoflurane or 100 mg/kg Ketamine and 10 mg/kg Xylazine. Tumor sizes
307 were measured twice weekly one week after inoculation. When the largest tumor reached 150
308 mm^3 in volume, mice were fed doxycycline-containing food to induce shRNA expression, or
309 treated thrice weekly for three weeks with 50 mg/kg DMSO, 50 mg/kg GSK-J4
310 (Medchemexpress, NJ, USA), or 5 mg/kg doxorubicin (Fujifilm Wako Pure Chemical
311 Industries) intraperitoneally. Mice were euthanized with CO_2 when tumors reached 500 mm^3 in
312 volume or when mice exhibited abnormal behavior. Tumors and major organs were weighed and

313 fixed in 10% neutral buffered formalin for histological examination.

314

315 *4.4. Western Blotting*

316 SDS lysis buffer (2% SDS, 50 mM Tris-HCl [pH6.8], 1mM EDTA [pH 8.0]) with
317 EDTA-free proteinase inhibitor cocktail (Sigma-Aldrich, MO, USA) was added in cultured cells.
318 Cell lysates were then sonicated using BRANSON Sonifier 450 (Branson Ultrasonics
319 Corporation, CT, USA) for two secs. Protein concentrations were measured with the Pierce™
320 BCA Protein Assay Kit (Thermo Fisher Scientific) before adding 4X Sample loading buffer
321 (200 mM Tris-HCl buffer [pH 6.8], 8% SDS, 40% Glycerol, 1% bromophenol blue, 20%
322 2-mercaptoethanol) and denaturing at 98°C for 10 mins. 3 μg proteins were separated by
323 SDS-PAGE and electrotransferred onto Immobilon®-P transfer membranes (Merck Millipore,
324 MA, USA), blocked with 5% skim milk in Tris-buffered saline with 5% Tween 20 (TBST), or
325 5% BSA in TBST for 1 hour at room temperature (RT) and incubated with primary antibody in
326 Can Get Signal Solution® 1 (TOYOBO, Osaka, Japan) overnight at 4°C. The membranes were
327 washed with TBST three times before incubating with the corresponding secondary anti-mouse
328 or anti-rabbit IgG antibody (GE Healthcare) in Can Get Signal Solution® 2 (TOYOBO). Signals
329 were developed with Immobilon® Western Chemiluminescent HRP substrate (Merck Millipore)
330 and visualized in ImageQuant LAS 4000 mini luminescent image analyzer (GE Healthcare).

331 Captured data were processed using ImageJ software (Schneider et al., 2012). The list of
332 antibodies used in this study can be found as Table S1.
333
334 *4.5. Quantitative RT-PCR (qRT-PCR)*
335 Total RNA was extracted with Nucleospin® RNA isolation kit (Macherey-Nagel
336 GmbH & Co. Düren, Germany) following the manufacturer's instructions. Synthesis of cDNA
337 was performed using the PrimeScript™ Reverse Transcriptase (Takara Bio, Inc.) according to
338 the manufacturer's instructions. qRT-PCR was performed with StepOne™ Real Time System
339 (Thermo Fisher Scientific). The oligos for qRT-PCR were designed as described elsewhere
340 (Peters et al., 2007; Aoshima et al., 2018) and listed in Table S2.
341
342 *4.6. RNA-seq*
343 RNA-seq for CnAOEC or JuB2 to estimate gene expression of epigenetic regulators
344 were performed in monoplicate. RNA-seq for JuB2 expressing shRNA control and shKDM2B
345 were performed in triplicate. Upon reaching 80% confluency, RNA was extracted with
346 Nucleospin® RNA isolation kit (Macherey-Nagel GmbH & Co.) following the manufacturer's
347 instructions. RNA samples were submitted to Annoroad (Beijing, China) for further analyses.
348 Quality testing was carried by measuring RNA integrity (RIN), $OD_{260/280,}$ and $OD_{260/230}$. All

samples had an RIN of 9.3 or better and OD readings were within the range of 1.8–2.2. RNA-seq libraries were constructed using NEBNext® Ultra RNA Library Prep Kit for llumina® (New England Biolabs, MA, USA) and sequenced with the Illumina HiSeq X-Ten platform (Illumina, CA, USA) to generate a minimum of 20 million paired-end 150 bp reads. Sequencing reads were mapped to the canine reference genome CanFam3.1 using STAR and aligned using RSEM (Li and Dewey, 2011; Dobin et al., 2013). Differential expression analyses were carried out using edgeR (Robinson et al., 2009), and gene expression profiles were analyzed by GSEA v4.03 (Mootha et al., 2003; Subramanian et al., 2005). The gene set database of h. all. v7.1. symbols. gmt (Hallmarks) was used.

4.7. shRNA vector construction

The shRNAs used in this study were designed using the Hannon lab shRNA design tool (http://hannonlab.cshl.edu/GH_shRNA.html, Cold Spring Harbor Laboratory). Oligos were inserted to pLKO.1-TRC or pInducer10-mir-RUP-PheS vector, a gift from David Root (Addgene plasmid # 10878; http://n2t.net/addgene:10878; RRID:Addgene_10878) (Moffat et al., 2006) and from Stephen Elledge (Addgene plasmid # 44011; http://n2t.net/addgene:44011; RRID:Addgene 44011) (Meerbrey et al., 2011), respectively. shRNA expressions were induced by supplementing 2 μM doxycycline in the culture medium. The list of oligonucleotide

367 sequences used for shRNA knockdown can be found as Table S3.

368

369 *4.8. Overexpression vector construction*

370 The coding sequence of canine *KDM2B* (ENSCAFT00000093772.1) was cloned from
371 cDNA synthesized from the canine heart. Mutant KDM2B (H283Y, C586A, ΔPHD) were
372 synthesized as described elsewhere (Edelheit et al., 2009). The amplicon tagged with FLAG
373 sequences at its 3' end was ligated into CSII-CMV-MCS-IRES2-Bsd vector, a gift from Dr.
374 Miyoshi (RIKEN BioResource Center, Ibaraki, Japan), with In-Fusion® HD Cloning Kit (Takara
375 Bio, Inc.) according to the manufacturer's instruction. The list of oligonucleotide sequences
376 used for CDS cloning are can be found as Table S4.

377

378 *4.9. Lentivirus production*

379 Lentiviruses were produced following a protocol described elsewhere with a slight
380 modification in which virus containing culture medium was used directly without concentrating
381 the lentiviruses (Aoshima et al., 2018). Selection of positive clones was done by culturing of
382 cells in 10 μg/ml blasticidin- or 4 μg/ml puromycin-containing cell medium.

383

384 *4.10. Alkaline comet assay*

JuB2 overexpressing shRNA for *KDM2B* or scrRNA were cultured in doxycycline-containing medium for four days. 4×10^4 cells were used for alkaline comet assay as described previously (Morita et al., 2019). 20 μg/mL PI was used for staining and the comets were visualized with BZ-9000 (BIOREVO) fluorescence microscope (Keyence, Osaka, Japan). Experiments were performed at least three times with triplicates.

4.11. Cell cycle analysis

HSA cells were stained with 1 μL of 0.1M BrdU for 45 mins at 37°C upon reaching 70% confluency. Cells were washed with phosphate-buffered saline (PBS) and trypsinized routinely. Afterwards, cells were fixed in 70% ethanol overnight and washed with 0.5% Triton X-100 in PBS (PBST) before resuspending the cells in 500 μL of 2N HCl-0.5% Triton X-100 for 30 mins at RT and neutralizing with 500 μL of 0.1M $Na_2B_4O_7 \cdot 10H_2O$ (pH 8.5) for 30 mins at RT. Then, cells were blocked with 1% BSA-0.3% Triton X-100 in PBS for 1 hr and were counted and divided into two tubes; 2.5×10^5 cells were used as controls and incubated in the blocking buffer while 6×10^5 cells were incubated with anti-BrdU monoclonal antibody (1:100; MOBU-1 clone, B35128, Thermo Fisher Scientific) for 1 hr at RT. Excess primary antibodies were washed before staining with AlexaFluor 488 (1:1000; Thermo Fisher Scientific). DNA was stained with 10 μg/200 μL Propidum Iodide (Dojindo Molecular Technologies, Inc., Kumamoto,

403 Japan). Cell cycle and proliferation were analyzed in BD FACSVerse™ flow cytometer (BD
404 Biosciences, NJ, USA). Results were analyzed with FCS Express 4 software (De Novo
405 Software, CA, USA). Experiments were performed at least three times with triplicates.
406
407 *4.12. Cell viability analysis*
408 Cell viability was measured with Cell Counting Kit-8 (Dojindo Molecular
409 Technologies, Inc.) according to the manufacturer's instructions. The absorbance at 450 nm was
410 measured with NanoDrop™ 2000 (Thermo Fisher Scientific). Determination of IC_{50} was
411 performed using Ky Plot 6.0 software (KyensLab, Inc., Tokyo, Japan) as described elsewhere
412 (Morita et al., 2019). Experiments were performed at least three times with triplicates.
413
414 *4.13. Colony formation assay*
415 500 HSA cells were seeded in 6-well culture plates containing 2 mL normal medium
416 supplemented with DMSO or 2 μM doxycycline. Cells were cultured until the largest colony
417 reached 2 mm in diameter. Cells were fixed with 4% paraformaldehyde for 20 mins at RT and
418 stained with 0.01% Crystal Violet (Sigma-Aldrich, MO, USA) for 30 mins at RT. Images were
419 captured with ChemiDoc XRS Plus (Bio-rad, CA, USA). Colony areas were measured using
420 ColonyArea plugin for ImageJ (Schneider et al., 2012; Guzmán et al., 2014). Experiments were

421 performed at least three times with triplicates.

422

423 *4.14. Cleavage Under Target & Release Using Nuclease (CUT&RUN)*

424 We used CUT&RUN Assay Kit (#86652, Cell Signaling Technology, MA, USA) for
425 CUT&RUN assay according to the manufacturer's instruction followed by qRT-PCR with
426 StepOne™ Real Time System (Thermo Fisher Scientific). Results were normalized by Ct values
427 of IgG isotype control samples. The oligos for qRT-PCR were listed in Table S5.

428

429 *4.15. Histopathology and immunohistochemistry (IHC)*

430 Tumor samples were obtained from patients with written informed consents of the
431 owners. Hematoxylin and eosin staining was performed as previously described (Maharani et al.,
432 2018). For IHC, heat-induced antigen retrieval was performed in citric acid buffer (pH 6.8) in a
433 pressure cooker for 10 mins. Endogenous peroxidases were quenched with 0.3% H_2O_2 in
434 methanol for 15 min at RT before blocking the tissue sections with 10% normal rabbit serum
435 (Nichirei biosciences, Tokyo, Japan) for an hour at RT. Tissue sections were incubated with
436 KDM2B antibody (sc-293279, 1:50, Santa Cruz Biotechnology, CA, USA) overnight at 4°C.
437 Slides were washed with 0.01M PBS before incubating with rabbit anti-mouse antibody
438 (Nichirei biosciences) for 30 min at RT. Signals were developed with 3,3'-diaminobenzidine

tetrahydrochloride (DAB; Dojindo).

4.16. Quantification of IHC scores

Histological slides were scanned with Nano Zoomer 2.0-RS (Hamamatsu Photonics, Hamamatsu, Japan) and processed in QuPath ver 0.2.1 (Bankhead et al., 2017). Scanned slides were opened as Brightfield (H-DAB) in QuPath, and staining colors were automatically adjusted using Estimate Stain Vectors function. Healthy tumor regions or normal blood vessels were randomly selected, and cells were detected using Cell Detection function. Cells were annotated based on their morphologies and location to allow QuPath to automatically classify each cell type correctly using the Create Detection Classifiers function. The measured data was exported and used for further analyses. KDM2B signals were found only in heterochromatin regions in nuclei but the nuclei also had abundant euchromatin region. Furthermore, nonspecific signals from fibrin and erythrocytes can often be classified by the software as nuclear or cytoplasmic signal in endothelial cells. Therefore, to make the analysis as precise as possible, we used Nuclear: DAB OD max scores for quantitative analysis.

4.17. Statistical analysis

Statistical analyses were performed with Microsoft Excel and R software (version

3.6.3). Student's *t*-tests was used to analyze the difference between two groups while Tukey's test was used to analyze differences between multiple groups. The significance of the differences in tumor volumes of DMSO, GSK-J4 or doxorubicin-treated mice were compared using Dunnet's test while their survival post-treatment were compared using Log-rank test. *P*-values less than 0.05 were considered statistically significant.

CRediT authorship contribution statement

Kevin Christian Montecillo Gulay: Conceptualization, Methodology, Formal analysis, Investigation, Data Curation, Writing - Original Draft, Writing - Review & Editing, Funding acquisition. **Keisuke Aoshima**: Conceptualization, Methodology, Formal analysis, Investigation, Data Curation, Writing - Review & Editing, Supervision, Funding acquisition. **Yuki Shibata**: Methodology, Investigation. **Hironobu Yasui**: Methodology, Investigation. **Qin Yan**: Methodology, Writing - Review & Editing, Supervision. **Atsushi Kobayashi**: Writing - Review & Editing. **Takashi Kimura**: Supervision.

Acknowledgements

We are grateful to Dr. Osamu Ichii, Dr. Junpei Yamazaki, and Dr. Noboru Sasaki for their invaluable support during the conduct of the study. We appreciate useful discussions with

the members of the Laboratory of Comparative Pathology, Faculty of Veterinary Medicine, Hokkaido University, and the members of Yan laboratory, Department of Pathology, Yale School of Medicine. This research was supported by the Sasakawa Scientific Research Grant from the Japan Science Society (KG, Research No. 2019-4111) provided by the Japan Science Society and the KAKENHI Grant-in-Aid for Young Scientist (KA, Number 18K14575 and 20K15654) provided by Japan Society for the Promotion of Science.

Availability of data and materials

The RNA sequence data was deposited on NCBI's Gene Expression Omnibus (GSE166540). All other data supporting the findings of this study can be found within the supplementary files.

Preprint

This paper has been uploaded on bioRxiv as a preprint (doi: https://doi.org/10.1101/2020.11.17.387704).

References

Aoshima, K., Fukui, Y., Gulay, K.C.M., Erdemsurakh, O., Morita, A., Kobayashi, A., Kimura, T., 2018. Notch2 signal is required for the maintenance of canine hemangiosarcoma cancer stem cell-like cells. BMC Vet. Res. 14, 301.

Bankhead, P., Loughrey, M.B., Fernández, J.A., Dombrowski, Y., McArt, D.G., Dunne, P.D., McQuaid, S., Gray, R.T., Murray, L.J., Coleman, H.G., *et al*., 2017. QuPath: Open source software for digital pathology image analysis. Sci. Rep. 7, 16878.

Batschinski, K., Nobre, A., Vargas-Mendez, E., Tedardi, M. V., Cirillo, J., Cestari, G., Ubukata, R., Dagli, M.L.Z., 2018. Canine visceral hemangiosarcoma treated with surgery alone or surgery and doxorubicin: 37 cases (2005-2014). Can. Vet. J. 59, 967–972.

Brzostek-Racine, S., Gordon, C., Van Scoy, S., Reich, N.C., 2011. The DNA damage response induces IFN. J. Immunol. 187, 5336–5345.

Carvalho, C., Santos, R., Cardoso, S., Correia, S., Oliveira, P., Santos, M., Moreira, P., 2009. Doxorubicin: The Good, the Bad and the ugly effect. Curr. Med. Chem. 16, 3267–3285.

Chen, J., Harding, S.M., Natesan, R., Tian, L., Benci, J.L., Li, W., Minn, A.J., Asangani, I.A., Greenberg, R.A., 2020. Cell cycle checkpoints cooperate to suppress DNA- and RNA-associated molecular pattern recognition and anti-tumor immune responses. Cell Rep. 32, 108080.

510 Chen, L., Fu, L., Kong, X., Xu, J., Wang, Z., Ma, X., Akiyama, Y., Chen, Y., Fang, J., 2014.
511 Jumonji domain-containing protein 2B silencing induces DNA damage response via
512 STAT3 pathway in colorectal cancer. Br. J. Cancer. 110, 1014–1026.
513 Clifford, C.A., Mackin, A.J., Henry, C.J., 2000. Treatment of canine hemangiosarcoma: 2000
514 and beyond. J. Vet. Intern. Med. 14, 479–485.
515 Dobin, A., Davis, C.A., Schlesinger, F., Drenkow, J., Zaleski, C., Jha, S., Batut, P., Chaisson, M.,
516 Gingeras, T.R., 2013. STAR: Ultrafast universal RNA-seq aligner. Bioinformatics 29,
517 15–21.
518 Edelheit, O., Hanukoglu, A., Hanukoglu, I., 2009. Simple and efficient site-directed
519 mutagenesis using two single-primer reactions in parallel to generate mutants for protein
520 structure-function studies. BMC Biotechnol. 9, 61.
521 Fosmire, S.P., Dickerson, E.B., Scott, A.M., Bianco, S.R., Pettengill, M.J., Meylemans, H.,
522 Padilla, M., Frazer-Abel, A.A., Akhtar, N., Getzy, D.M., *et al.,* 2004. Canine malignant
523 hemangiosarcoma as a model of primitive angiogenic endothelium. Lab. Investig. 84,
524 562–572.
525 Guzmán, C., Bagga, M., Kaur, A., Westermarck, J., Abankwa, D., 2014. ColonyArea: An
526 ImageJ plugin to automatically quantify colony formation in clonogenic assays. PLoS One
527 9, e92444.

528 Han, X.R., Zha, Z., Yuan, H.X., Feng, X., Xia, Y.K., Lei, Q.Y., Guan, K.L., Xiong, Y., 2016.
529 KDM2B/FBXL10 targets c-Fos for ubiquitylation and degradation in response to
530 mitogenic stimulation. Oncogene 35, 4179–4190.
531 Harasawa, R., Mizusawa, H., Fujii, M., Yamamoto, J., Mukai, H., Uemori, T., Asada, K., Kato,
532 I., 2005. Rapid detection and differentiation of the major mycoplasma contaminants in cell
533 cultures using real-time PCR with SYBR green I and melting curve analysis. Microbiol.
534 Immunol. 49, 859–863.
535 Harasawa, R., Mizusawa, H., Nozawa, K., Nakagawa, T., Asada, K., Kato, I., 1993. Detection
536 and tentative identification of dominant mycoplasma species in cell cultures by restriction
537 analysis of the 16S-23S rRNA intergenic spacer regions. Res. Microbiol. 144, 489–493.
538 He, J., Nguyen, A.T., Zhang, Y., 2011. KDM2B/JHDM1b, an H3K36me2-specific demethylase,
539 is required for initiation and maintenance of acute myeloid leukemia. Blood 117,
540 3869–3880.
541 Heinemann, B., Nielsen, J.M., Hudlebusch, H.R., Lees, M.J., Larsen, D.V., Boesen, T., Labelle,
542 M., Gerlach, L.O., Birk, P., Helin, K., 2014. Inhibition of demethylases by GSK-J1/J4.
543 Nature 514, E1–E2.
544 Hong, X., Xu, Y., Qiu, X., Zhu, Y., Feng, X., Ding, Z., Zhang, S., Zhong, L., Zhuang, Y., Su, C.,
545 *et al.,* 2016. MiR-448 promotes glycolytic metabolism of gastric cancer by downregulating

546 KDM2B. Oncotarget 7, 22092–22102.

547 Kim, J., Graef, A.J., Dickerson, E.B., Modiano, J.F., 2015. Pathobiology of Hemangiosarcoma

548 in Dogs: Research Advances and Future Perspectives. Vet. Sci. 2, 388–405.

549 Kottakis, F., Foltopoulou, P., Sanidas, I., Keller, P., Wronski, A., Dake, B.T., Ezell, S.A., Shen,

550 Z., Naber, S.P., Hinds, P.W., *et al.,* 2014. NDY1/KDM2B functions as a master regulator

551 of polycomb complexes and controls self-renewal of breast cancer stem cells. Cancer Res.

552 74, 3935–3946.

553 Kottakis, F., Polytarchou, C., Foltopoulou, P., Sanidas, I., Kampranis, S.C., Tsichlis, P.N., 2011.

554 FGF-2 Regulates Cell Proliferation, Migration, and Angiogenesis through an

555 NDY1/KDM2B-miR-101-EZH2 Pathway. Mol. Cell 43, 285–298.

556 Kurt, I.C., Sur, I., Kaya, E., Cingoz, A., Kazancioglu, S., Kahya, Z., Toparlak, O.D.,

557 Senbabaoglu, F., Kaya, Z., Ozyerli, E., *et al.,* 2017. KDM2B, an H3K36-specific

558 demethylase, regulates apoptotic response of GBM cells to TRAIL. Cell Death Dis. 8,

559 e2897.

560 Li, B., Dewey, C.N., 2011. RSEM: Accurate transcript quantification from RNA-Seq data with

561 or without a reference genome. BMC Bioinformatics 12, 323.

562 Li, Y., Zhang, M., Sheng, M., Zhang, P., Chen, Z., Xing, W., Bai, J., Cheng, T., Yang, F.C., Zhou,

563 Y., 2018. Therapeutic potential of GSK-J4, a histone demethylase KDM6B/JMJD3

564 inhibitor, for acute myeloid leukemia. J. Cancer Res. Clin. Oncol. 144, 1065–1077.

565 Maharani, A., Aoshima, K., Onishi, S., Gulay, K.C.M., Kobayashi, A., Kimura, T., 2018.

566 Cellular atypia is negatively correlated with immunohistochemical reactivity of CD31 and

567 vWF expression levels in canine hemangiosarcoma. J. Vet. Med. Sci. 80, 213–218.

568 Mboko, W.P., Mounce, B.C., Wood, B.M., Kulinski, J.M., Corbett, J.A., Tarakanova, V.L., 2012.

569 Coordinate Regulation of DNA Damage and Type I Interferon Responses Imposes an

570 Antiviral State That Attenuates Mouse Gammaherpesvirus Type 68 Replication in Primary

571 Macrophages. J. Virol. 86, 6899–6912.

572 Meerbrey, K.L., Hu, G., Kessler, J.D., Roarty, K., Li, M.Z., Fang, J.E., Herschkowitz, J.I.,

573 Burrows, A.E., Ciccia, A., Sun, T., *et al.,* 2011. The pINDUCER lentiviral toolkit for

574 inducible RNA interference in vitro and in vivo. Proc. Natl. Acad. Sci. U. S. A. 108,

575 3665–3670.

576 Megquier, K., Turner-Maier, J., Swofford, R., Kim, J.H., Sarver, A.L., Wang, C., Sakthikumar,

577 S., Johnson, J., Koltookian, M., Lewellen, M., *et al.,* 2019. Comparative genomics reveals

578 shared mutational landscape in canine hemangiosarcoma and human angiosarcoma. Mol.

579 Cancer Res. 17, 2410–2421.

580 Moffat, J., Grueneberg, D.A., Yang, X., Kim, S.Y., Kloepfer, A.M., Hinkle, G., Piqani, B.,

581 Eisenhaure, T.M., Luo, B., Grenier, J.K., *et al.,* 2006. A Lentiviral RNAi Library for

582 Human and Mouse Genes Applied to an Arrayed Viral High-Content Screen. Cell 124,
583 1283–1298.
584 Moosavi, A., Ardekani, A.M., 2016. Role of epigenetics in biology and human diseases. Iran
585 Biomed. J. 20, 246–258.
586 Mootha, V.K., Lindgren, C.M., Eriksson, K.F., Subramanian, A., Sihag, S., Lehar, J., Puigserver,
587 P., Carlsson, E., Ridderstråle, M., Laurila, E., *et al.,* 2003. PGC-1α-responsive genes
588 involved in oxidative phosphorylation are coordinately downregulated in human diabetes.
589 Nat. Genet. 34, 267–273.
590 Morita, A., Aoshima, K., Gulay, K.C.M., Onishi, S., Shibata, Y., Yasui, H., Kobayashi, A.,
591 Kimura, T., 2019. High drug efflux pump capacity and low DNA damage response induce
592 doxorubicin resistance in canine hemangiosarcoma cell lines. Res. Vet. Sci. 127, 1–10.
593 Murai, A., Asa, S., Kodama, A., Hirata, A., Yanai, T., Sakai, H., 2012. Constitutive
594 phosphorylation of the mTORC2/Akt/4E-BP1 pathway in newly derived canine
595 hemangiosarcoma cell lines. BMC Vet. Res. 8, 128.
596 Odom, A.L., Hatwig, C.A., Stanley, J.S., Benson, A.M., 1992. Biochemical determinants of
597 Adriamycin toxicity in mouse liver, heart and intestine. Biochem. Pharmacol. 43,
598 831–836.
599 Peta, E., Sinigaglia, A., Masi, G., Di Camillo, B., Grassi, A., Trevisan, M., Messa, L., Loregian,

600 A., Manfrin, E., Brunelli, M., *et al.,* 2018. HPV16 E6 and E7 upregulate the histone lysine
601 demethylase KDM2B through the c-MYC/miR-146a-5p axys. Oncogene 37, 1654–1668.
602 Peters, I.R., Peeters, D., Helps, C.R., Day, M.J., 2007. Development and application of multiple
603 internal reference (housekeeper) gene assays for accurate normalisation of canine gene
604 expression studies. Vet. Immunol. Immunopathol. 117, 55–66.
605 Robinson, M.D., McCarthy, D.J., Smyth, G.K., 2009. edgeR: A Bioconductor package for
606 differential expression analysis of digital gene expression data. Bioinformatics 26,
607 139–140.
608 Schneider, C.A., Rasband, W.S., Eliceiri, K.W., 2012. NIH Image to ImageJ: 25 years of image
609 analysis. Nat. Methods 9, 671–675.
610 Sharma, S., Kelly, T.K., Jones, P.A., 2009. Epigenetics in cancer. Carcinogenesis. 31, 27-36.
611 Sheltzer, J.M., Blank, H.M., Pfau, S.J., Tange, Y., George, B.M., Humpton, T.J., Brito, I.L.,
612 Hiraoka, Y., Niwa, O., Amon, A., 2011. Aneuploidy drives genomic instability in yeast.
613 Science 333, 1026–1030.
614 Stokes, M.P., Rush, J., MacNeill, J., Jian, M.R., Sprott, K., Nardone, J., Yang, V., Beausoleil,
615 S.A., Gygi, S.P., Livingstone, M., *et al.,* 2007. Profiling of UV-induced ATM/ATR
616 signaling pathways. Proc. Natl. Acad. Sci. U. S. A. 104, 19855–19860.
617 Subramanian, A., Tamayo, P., Mootha, V.K., Mukherjee, S., Ebert, B.L., Gillette, M.A.,

618 Paulovich, A., Pomeroy, S.L., Golub, T.R., Lander, E.S., *et al.,* 2005. Gene set enrichment
619 analysis: A knowledge-based approach for interpreting genome-wide expression profiles.
620 Proc. Natl. Acad. Sci. U. S. A. 102, 15545–15550.
621 Thomas, R., Borst, L., Rotroff, D., Motsinger-Reif, A., Lindblad-Toh, K., Modiano, J.F., Breen,
622 M., 2014. Genomic profiling reveals extensive heterogeneity in somatic DNA copy
623 number aberrations of canine hemangiosarcoma. Chromosom. Res. 22, 305–319.
624 Tzatsos, A., Pfau, R., Kampranis, S.C., Tsichlis, P.N., 2009. Ndy1/KDM2B immortalizes mouse
625 embryonic fibroblasts by repressing the lnk4a/Arf locus. Proc. Natl. Acad. Sci. U. S. A.
626 106, 2641–2646.
627 van den Boom, V., Maat, H., Geugien, M., Rodríguez López, A., Sotoca, A.M., Jaques, J.,
628 Brouwers-Vos, A.Z., Fusetti, F., Groen, R.W.J., Yuan, H., *et al.,* 2016. Non-canonical
629 PRC1.1 Targets Active Genes Independent of H3K27me3 and Is Essential for
630 Leukemogenesis. Cell Rep. 14, 332–346.
631 Wang, T., Chen, K., Zeng, X., Yang, J., Wu, Y., Shi, X., Qin, B., Zeng, L., Esteban, M.A., Pan,
632 G., *et al.,* 2011. The histone demethylases Jhdm1a/1b enhance somatic cell reprogramming
633 in a vitamin-C-dependent manner. Cell Stem Cell 9, 575–587.
634 Yan, M., Yang, X., Wang, H., Shao, Q., 2018. The critical role of histone lysine demethylase
635 KDM2B in cancer. Am. J. Transl. Res. 10, 2222–2233.

636 Yoshino, H., Ueda, T., Kawahata, M., Kobayashi, K., Ebihara, Y., Manabe, A., Tanaka, R., Ito,
637 M., Asano, S., Nakahata, T., *et al.,* 2000. Natural killer cell depletion by anti-asialo GM1
638 antiserum treatment enhances human hematopoietic stem cell engraftment in
639 NOD/Shi-scid mice. Bone Marrow Transplant 26, 1211–1216.
640 Zhu, J., Tsai, H.J., Gordon, M.R., Li, R., 2018. Cellular Stress Associated with Aneuploidy. Dev.
641 Cel. 44, 420–431.
642

643 **Figure legends**

644 **Fig. 1. Epigenetic regulators are dysregulated in HSA.**

645 (**A**) Transcripts per million (TPM) scores of histone demethylases in CnAOEC and JuB2 HSA
646 cell lines. (**B**) qRT-PCR verification of select histone demethylases in CnAOEC and HSA cell
647 lines. (**C**) Western blotting for KDM1A, KDM2A, and KDM2B in CnAOEC and HSA cell lines.
648 (**D**) Quantitative analysis of KDM1A, KDM2A, and KDM2B protein expressions in CnAOEC
649 and HSA cell lines. Data are presented as mean values ± SD, standard deviation. ***, $P < 0.001$,
650 Tukey's test.

651

652 **Fig. 2. KDM2B is important for HSA cell survival *in vitro* and *in vivo*.**

653 (**A**) Western blotting of KDM2B to verify the silencing efficiency of shRNA vectors developed
654 for KDM2B. (**B**) Cell viability analysis after the induction of the inducible shRNA vector using
655 doxycycline. Data are presented as mean values ± SD. ***, $P < 0.001$, Two-way ANOVA. (**C**)
656 Colony formation assay of JuB2 cells after KDM2B silencing. (**D**) Quantitative analysis of (C**)**.
657 N.D. means not detected. (**E**) Western blotting of histone modifications. (**F**) Cell viability
658 analysis after rescue overexpression of WT KDM2B, or dominant-negative mutants for the
659 JmjC ($KDM2B^{H283Y}$), CxxC ($KDM2B^{C586A}$), or PHD ($KDM2B^{\triangle PHD}$) domains. **, $P < 0.01$; ***,
660 $P < 0.001$, two-way ANOVA. (**G**) Tumor growth at different time points before and after the

induction of the shRNA expression in JuB2 cells inoculated in nude mice. ***, $P < 0.001$, two-way ANOVA with Dunnett's post-hoc test for tumor volumes after starting doxycycline treatments (arrow). (**H** and **I**) Tumor sizes (H) and weights (I) harboring scramble RNA or shRNA for KDM1A, KDM2A, or KDM2B 78 days after tumor transplantation. Scale bars, 1 cm. **, $P < 0.01$; ***, $P < 0.001$, Dunnett's test. Data are presented as mean values ± SD.

Fig. 3. KDM2B positively regulates DNA repair pathway.

(**A**) GSEA enrichment plot for UV_Response_DN in shKDM2B-A versus scrRNA-1. (**B**) qRT-PCR verification of gene expressions listed in UV_Response_DN gene set. (**C**) H2AK119ub1 and H3K4me3 enrichment at the promoters or gene bodies. Results are normalized by IgG control samples and indicated as fold change. Dotted lines indicate fold change =1. Data are presented as mean values ± SD.. *, $P < 0.05$; **, $P < 0.01$; *** $P < 0.001$, Dunnett's test. (**D** and **E**) Western blotting for ATM, c-FOS, and γH2A.X in normal endothelial cells and HSA cell lines (D) and in JuB2 cells expressing shRNA control or shKDM2B (E). In (D), KDM2B and Actin images are the same as Fig. 1C because we used the same samples. (**F**) Representative images of alkaline comet assays in JuB2 cells expressing shRNA control or shKDM2B. (**G**) Tail DNA percentages, lengths, and momentums of JuB2 HSA cells expressing shRNA control or shKDM2B Data are presented as mean values ± SD.. *** $P < 0.001$, Tukey's test.

Fig. 4. KDM2B regulates aneuploidy and apoptosis in HSA.

(**A**) Histograms of PI intensities in scrRNA and shKDM2B JuB2 cells. (**B**) Percentages of aneuploid cells in shRNA and shKDM2B JuB2 cells. ***, $P < 0.001$, Tukey's test. (**C**) Histograms of PI intensities in EV infected JuB2 cells and WT KDM2B JuB2 cells. (**D**) Percentages of aneuploid cells in EV JuB2 and WT KDM2B JuB2. ***, $P < 0.001$, Student-*t* test. (**E**) Western blotting for cleaved-caspase 3, BAX and ERK1/2 in JuB2 HSA cells expressing scrRNA controls or shKDM2B RNAs. KDM2B and Actin images are the same as Fig. 3E because we used the same samples.. (**F**) Western blotting of ERK1/2 in CnAOEC infected with EV or overexpressing WT KDM2B. (**G**) Quantification of KDM2B and phosphorylated ERK1/2 expression in EV infected or WT KDM2B expressing CnAOEC normalized with Actin and total ERK1/2, respectively. Data are presented as mean values ± SD. ***, $P < 0.001$, Student's *t*-test. (**H**) qRT-PCR analysis of cell cycle related genes after overexpression of WT KDM2B in normal endothelial cells. Data are presented as mean values ± SD. **, $P < 0.01$; ***, $P < 0.001$, Student's *t*-test.

Fig. 5. KDM2B can be used as a differential biomarker for HSA.

(**A**) Representative images of immunohistochemistry (IHC) for clinical HSA samples. Top: Normal endothelial cells (EC) in the healthy region. Bottom: HSA tumor cells in the tumor

699 region. Inserted pictures are magnified views and arrows indicate EC and tumor cells.
700 Proliferation patterns are indicated with case numbers. Scale bars, 100 μm. (**B**) Max nuclear
701 DAB intensities in individual endothelial cells (EC) and tumor cells (Tumor) of each HSA case.
702 (**C**) Average max nuclear DAB intensities of EC and tumor cells in each HSA case. Data are
703 presented as mean values ± SD. **, $P < 0.01$, Student's *t*-test. (**D**) Representative IHC images of
704 hemangioma (HMA), a benign endothelial cell tumor. Top: EC in the healthy region. Bottom:
705 HSA tumor cells in the tumor region. Inserted pictures are magnified views and arrows indicate
706 EC and tumor cells. Scale bars, 100 μm. (**E**) Max nuclear DAB intensities in individual EC and
707 tumor cells of each HMA case. (**F**) Average max nuclear DAB intensities of EC and tumor cells
708 in each HMA case. Data are presented as mean values ± SD. Student's *t*-test. (**G**) Comparison of
709 relative KDM2B intensity of HSA and HMA cells normalized by normal endothelial cells in
710 their respective slides. Data are presented as mean values ± SD. **, $P < 0.01$, Student's *t*-test.
711
712 **Fig. 6. GSK-J4 inhibits HSA cell proliferation *in vitro* and *in vivo*.**
713 (**A**) Survival rates and IC_{50} values of GSK-J4 or doxorubicin-treated HSA cell lines. (**B**)
714 Western blotting for γH2A.X, ATM and cleaved-caspase 3 in HSA cells treated with GSK-J4 or
715 doxorubicin. (**C**) Tumor growth curves of JuB2 HSA cell xenografts in nude mice. Treatment
716 with DMSO, GSK-J4, or doxorubicin started at day 45 (arrow). *n* indicates the number of
717 tumors. **, $P < 0.01$, two-way ANOVA with Dunnett's post-hoc test. (**D**) Gross images of

718 collected tumors at day 64. n indicates the number of collected tumors. **(E)** Tumor weights of
719 DMSO, GSK-J4, or doxorubicin-treated nude mice at necropsy. Data are presented as mean
720 values ± SD. *, $P < 0.05$; **, $P < 0.01$, Tukey's test. (**F**) Kaplan-Meier survival curves of
721 DMSO, GSK-J4, or doxorubicin-treated nude mice after starting treatments. **, $P < 0.01$,
722 Log-rank test. (**G**) Body weights of DMSO, GSK-J4, or doxorubicin-treated nude mice at
723 necropsy. Data are presented as mean values ± SD. **, $P < 0.01$, Tukey's test.
724

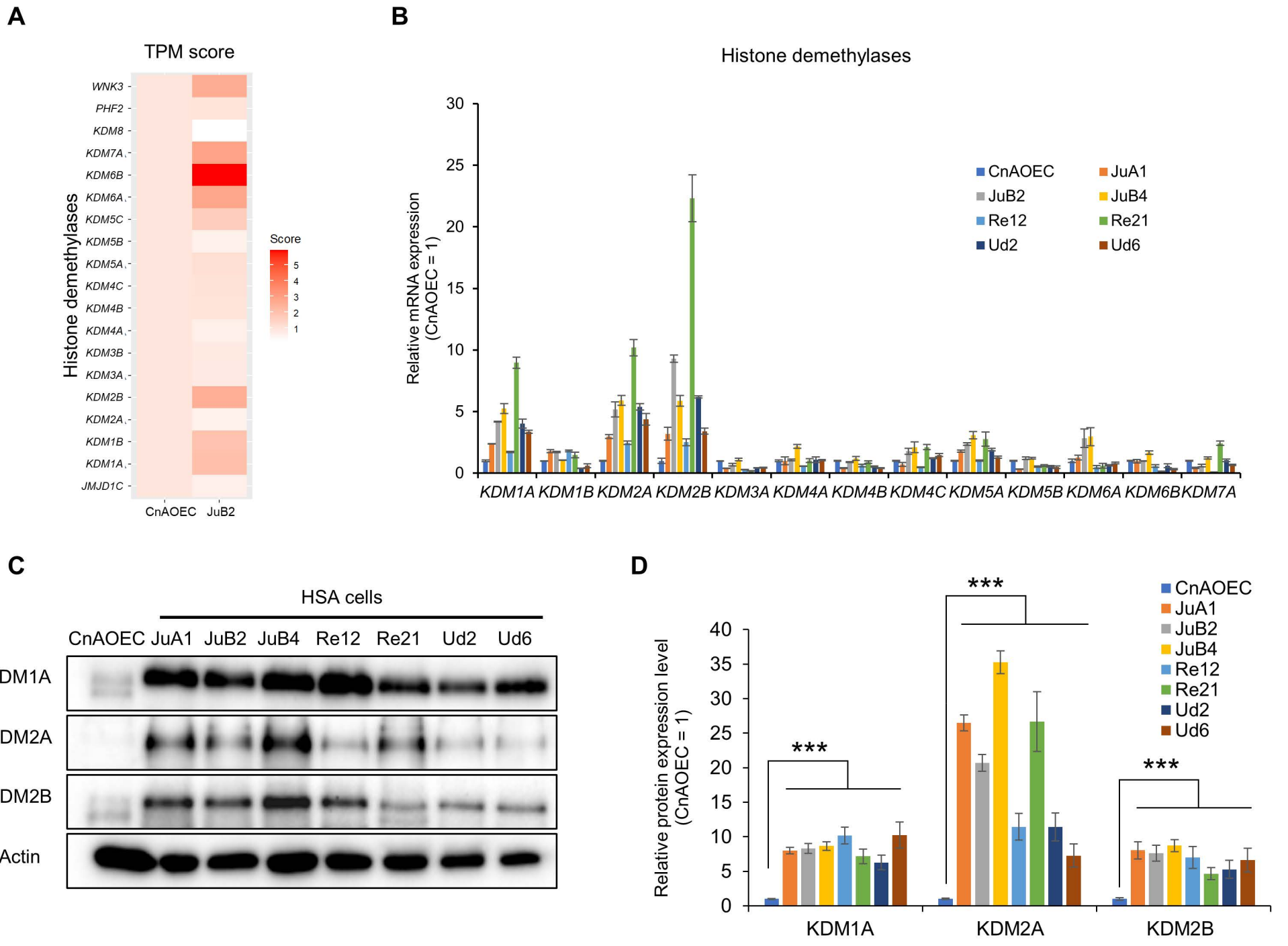
A
TPM score
Histone demethylases
WNK3
PHF2
KDM8
KDM7A
KDM6B
KDM6A
KDM5C
KDM5B
KDM5A
KDM4C
KDM4B
KDM4A
KDM3B
KDM3A
KDM2B
KDM2A
KDM1B
KDM1A
JMJD1C
CnAOEC
JuB2
Score
5
4
3
2
1
B
Histone demethylases
Relative mRNA expression (CnAOEC = 1)
30
25
20
15
10
5
0
CnAOEC
JuA1
JuB2
JuB4
Re12
Re21
Ud2
Ud6
KDM1A KDM1B KDM2A KDM2B KDM3A KDM4A KDM4B KDM4C KDM5A KDM5B KDM6A KDM6B KDM7A
C
HSA cells
CnAOEC JuA1 JuB2 JuB4 Re12 Re21 Ud2 Ud6
KDM1A
KDM2A
KDM2B
Actin
D
Relative protein expression level (CnAOEC = 1)
40
35
30
25
20
15
10
5
0
***
***
***
CnAOEC
JuA1
JuB2
JuB4
Re12
Re21
Ud2
Ud6
KDM1A
KDM2A
KDM2B

Fig. 1

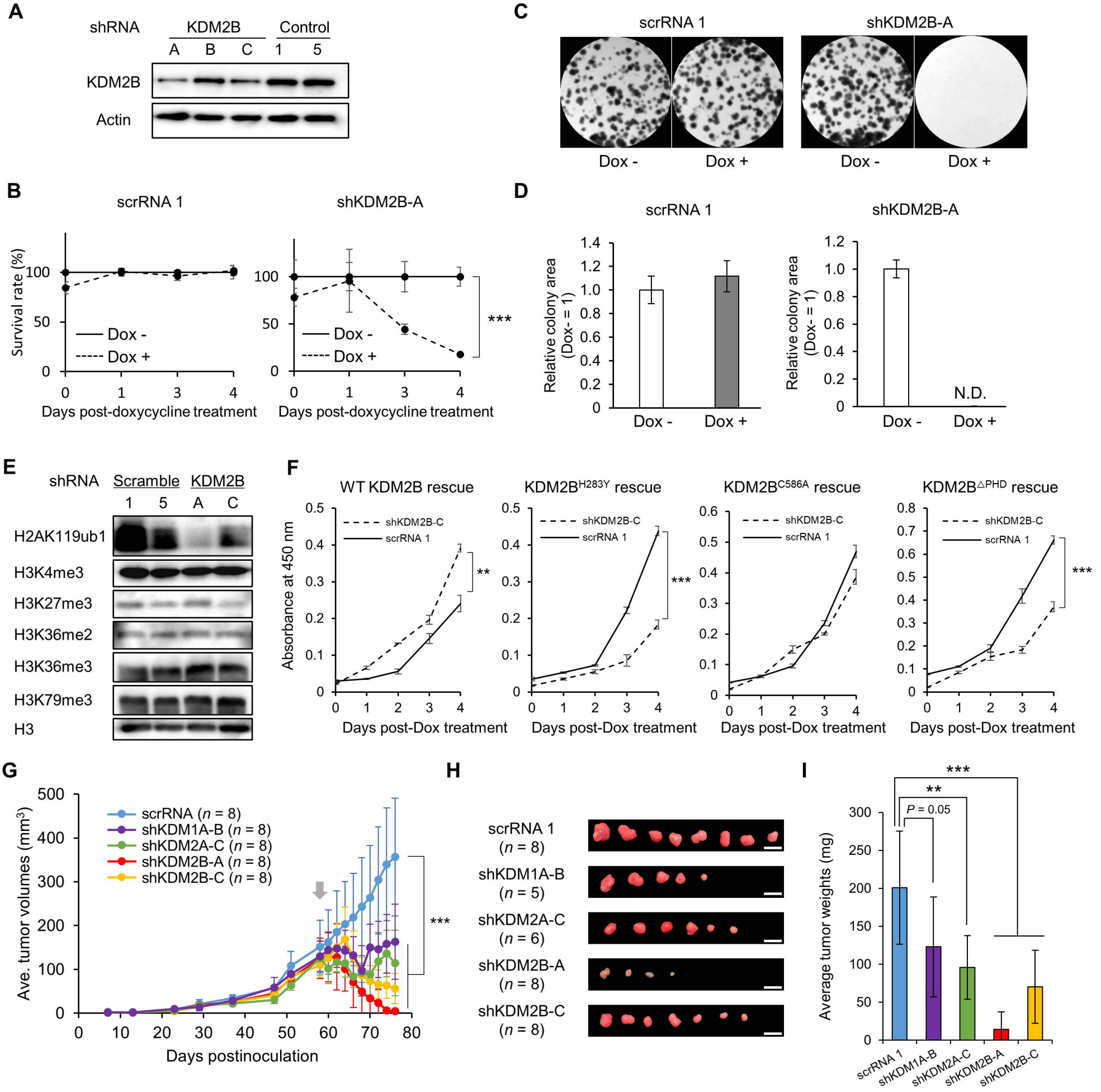
A
shRNA
KDM2B
Control
A B C 1 5
KDM2B
Actin
C
scrRNA 1
shKDM2B-A
Dox -
Dox +
B
Survival rate (%)
Dox -
Dox +
Days post-doxycycline treatment
***
D
Relative colony area (Dox- = 1)
N.D.
E
shRNA
Scramble
KDM2B
1 5 A C
H2AK119ub1
H3K4me3
H3K27me3
H3K36me2
H3K36me3
H3K79me3
H3
F
WT KDM2B rescue
KDM2B^H283Y rescue
KDM2B^C586A rescue
KDM2B^△PHD rescue
shKDM2B-C
scrRNA 1
Absorbance at 450 nm
Days post-Dox treatment
**
***
G
scrRNA (n = 8)
shKDM1A-B (n = 8)
shKDM2A-C (n = 8)
shKDM2B-A (n = 8)
shKDM2B-C (n = 8)
Ave. tumor volumes (mm3)
Days postinoculation
H
scrRNA 1 (n = 8)
shKDM1A-B (n = 5)
shKDM2A-C (n = 6)
shKDM2B-A (n = 8)
shKDM2B-C (n = 8)
I
Average tumor weights (mg)
P = 0.05
scrRNA 1
shKDM1A-B
shKDM2A-C
shKDM2B-A
shKDM2B-C

Fig. 2

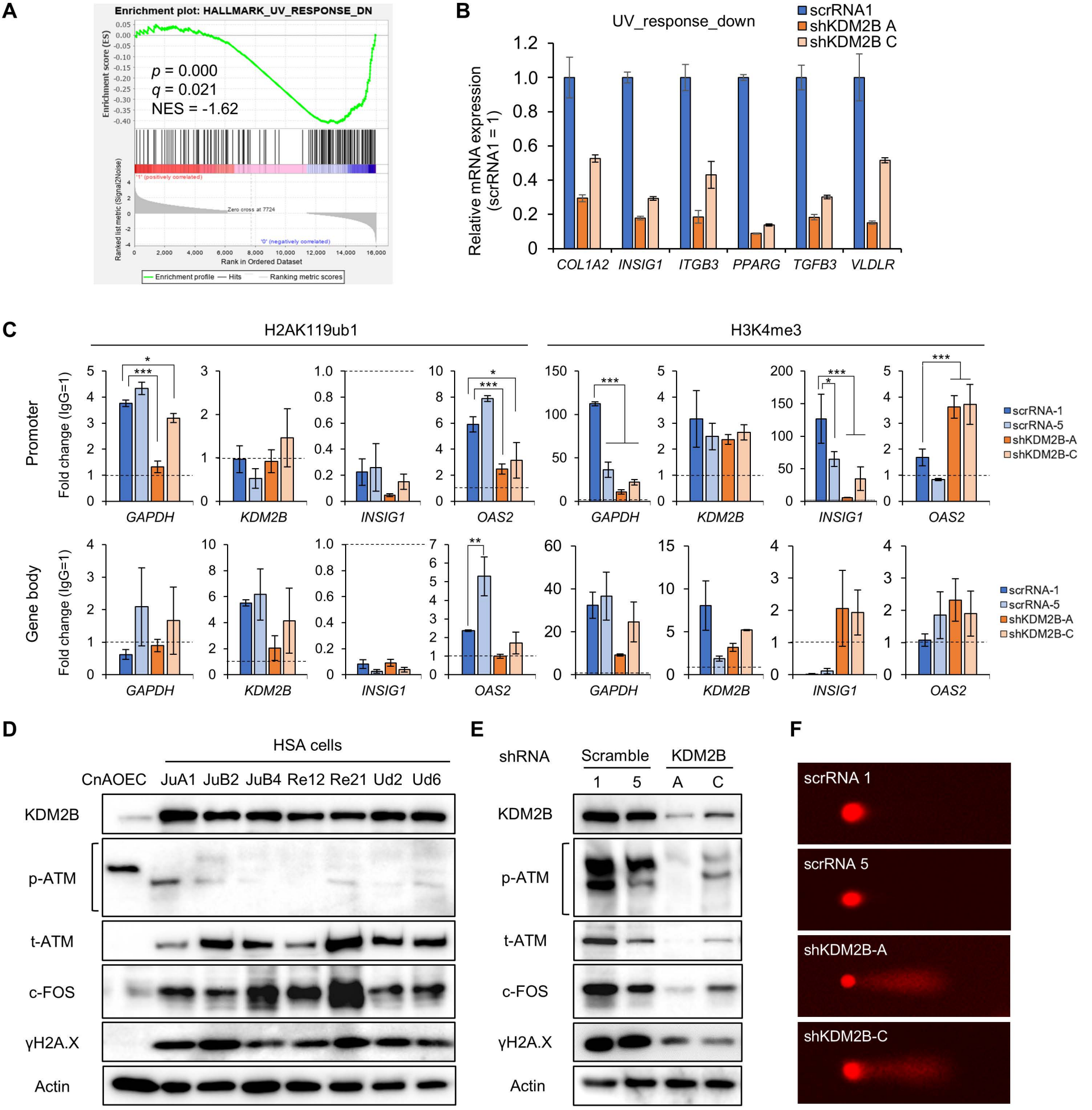
A
Enrichment plot: HALLMARK_UV_RESPONSE_DN
p = 0.000
q = 0.021
NES = -1.62
Enrichment score (ES)
Ranked list metric (Signal2Noise)
'1' (positively correlated)
Zero cross at 7724
'0' (negatively correlated)
Rank in Ordered Dataset
Enrichment profile
Hits
Ranking metric scores
B
UV_response_down
scrRNA1
shKDM2B A
shKDM2B C
Relative mRNA expression (scrRNA1 = 1)
COL1A2
INSIG1
ITGB3
PPARG
TGFB3
VLDLR
C
H2AK119ub1
H3K4me3
Promoter
Gene body
Fold change (IgG=1)
GAPDH
KDM2B
INSIG1
OAS2
scrRNA-1
scrRNA-5
shKDM2B-A
shKDM2B-C
D
HSA cells
CnAOEC
JuA1
JuB2
JuB4
Re12
Re21
Ud2
Ud6
KDM2B
p-ATM
t-ATM
c-FOS
γH2A.X
Actin
E
shRNA
Scramble
KDM2B
1
5
A
C
F
scrRNA 1
scrRNA 5
shKDM2B-A
shKDM2B-C
G
Tail DNA Percentages
%
Tail Lengths
pixels
Tail Momentums
pixels
scrRNA 1
scrRNA 5
shKDM2B-A
shKDM2B-C

Fig. 3

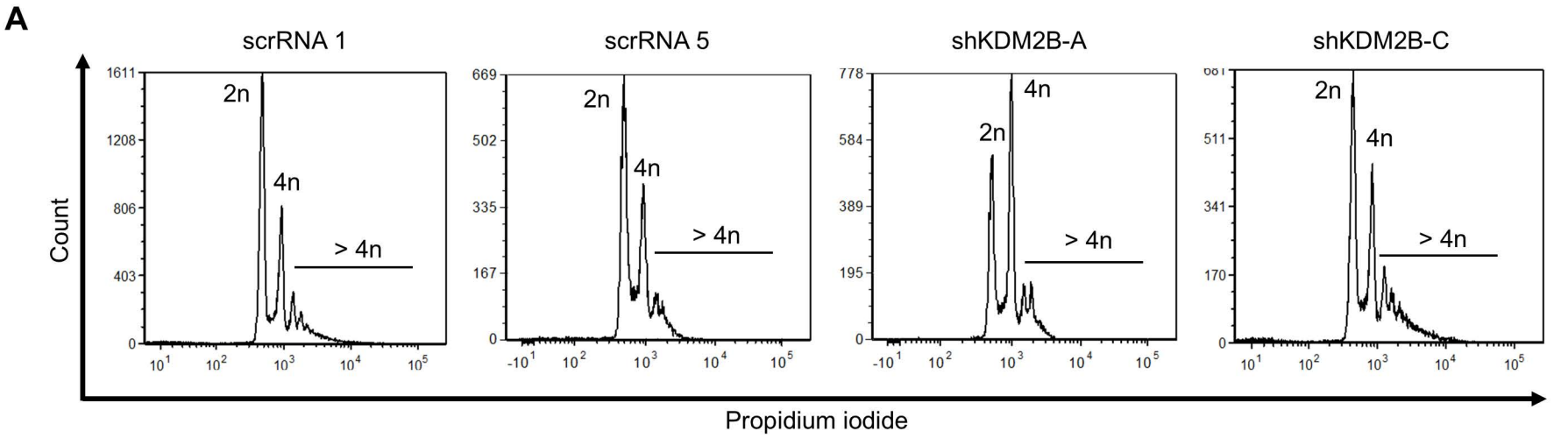
A
scrRNA 1
scrRNA 5
shKDM2B-A
shKDM2B-C
Count
2n
4n
> 4n
Propidium iodide

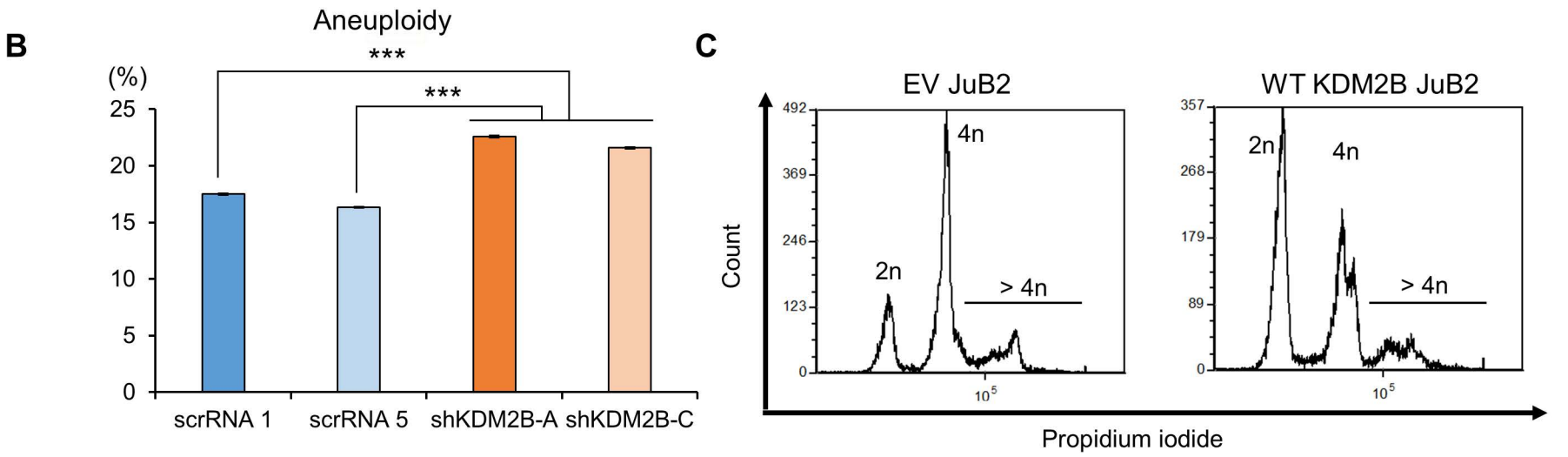
B
Aneuploidy
(%)
***
scrRNA 1
scrRNA 5
shKDM2B-A
shKDM2B-C
C
EV JuB2
WT KDM2B JuB2
Count
2n
4n
> 4n
Propidium iodide

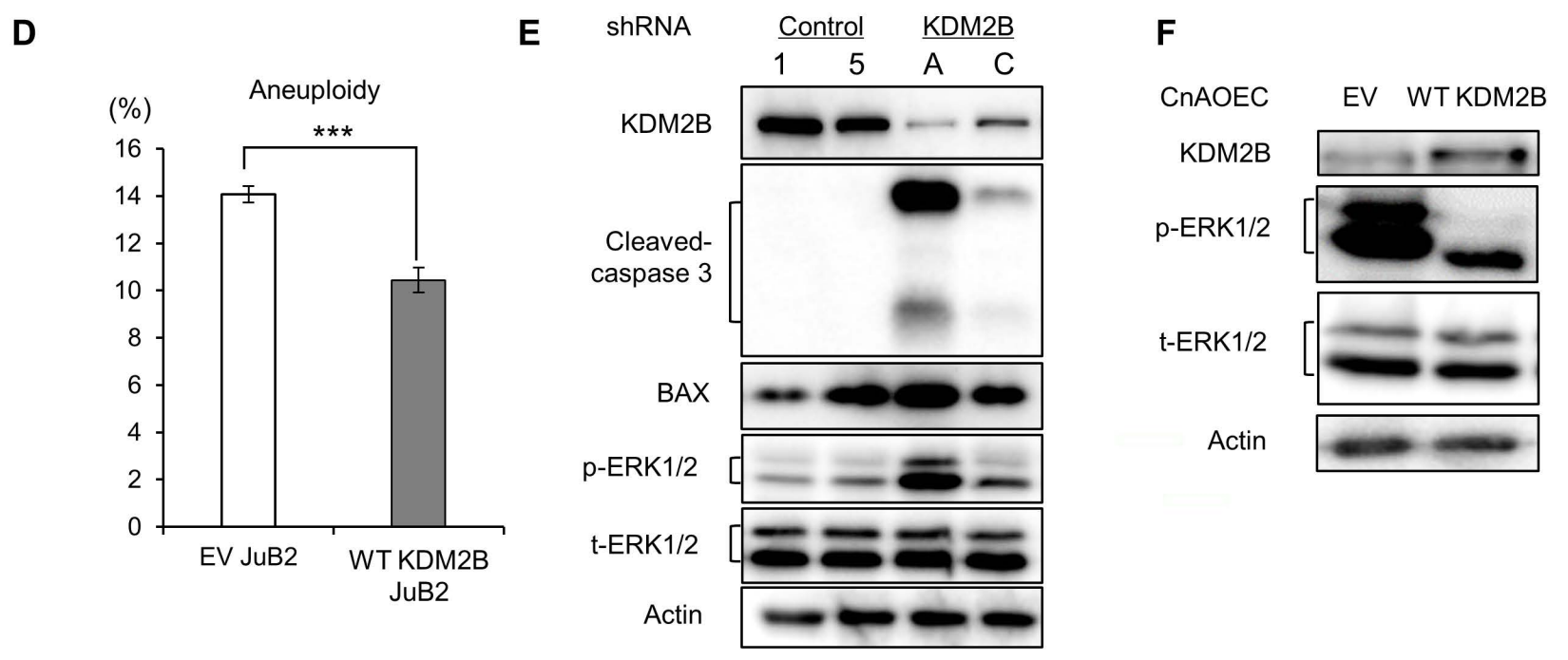
D
Aneuploidy
(%)
***
EV JuB2
WT KDM2B JuB2
E
shRNA
Control
KDM2B
1
5
A
C
KDM2B
Cleaved-caspase 3
BAX
p-ERK1/2
t-ERK1/2
Actin
F
CnAOEC
EV
WT KDM2B
KDM2B
p-ERK1/2
t-ERK1/2
Actin

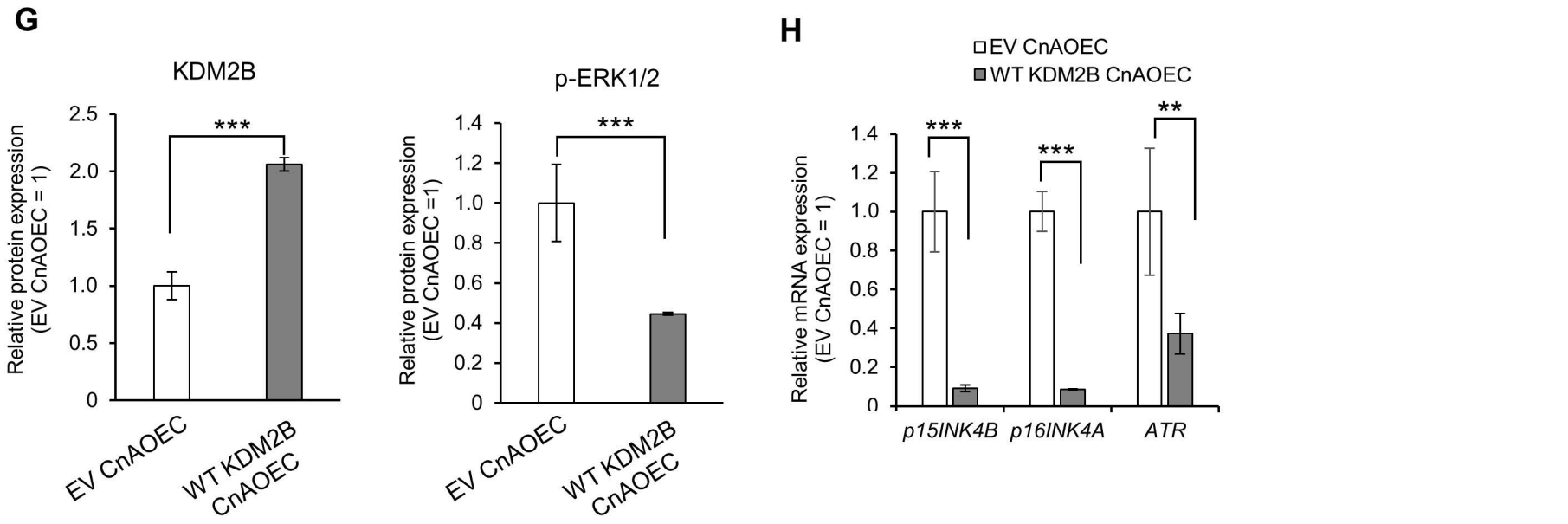
G
KDM2B
p-ERK1/2
Relative protein expression (EV CnAOEC = 1)
***
EV CnAOEC
WT KDM2B CnAOEC
H
EV CnAOEC
WT KDM2B CnAOEC
Relative mRNA expression (EV CnAOEC = 1)
**
p15INK4B
p16INK4A
ATR

Fig. 4

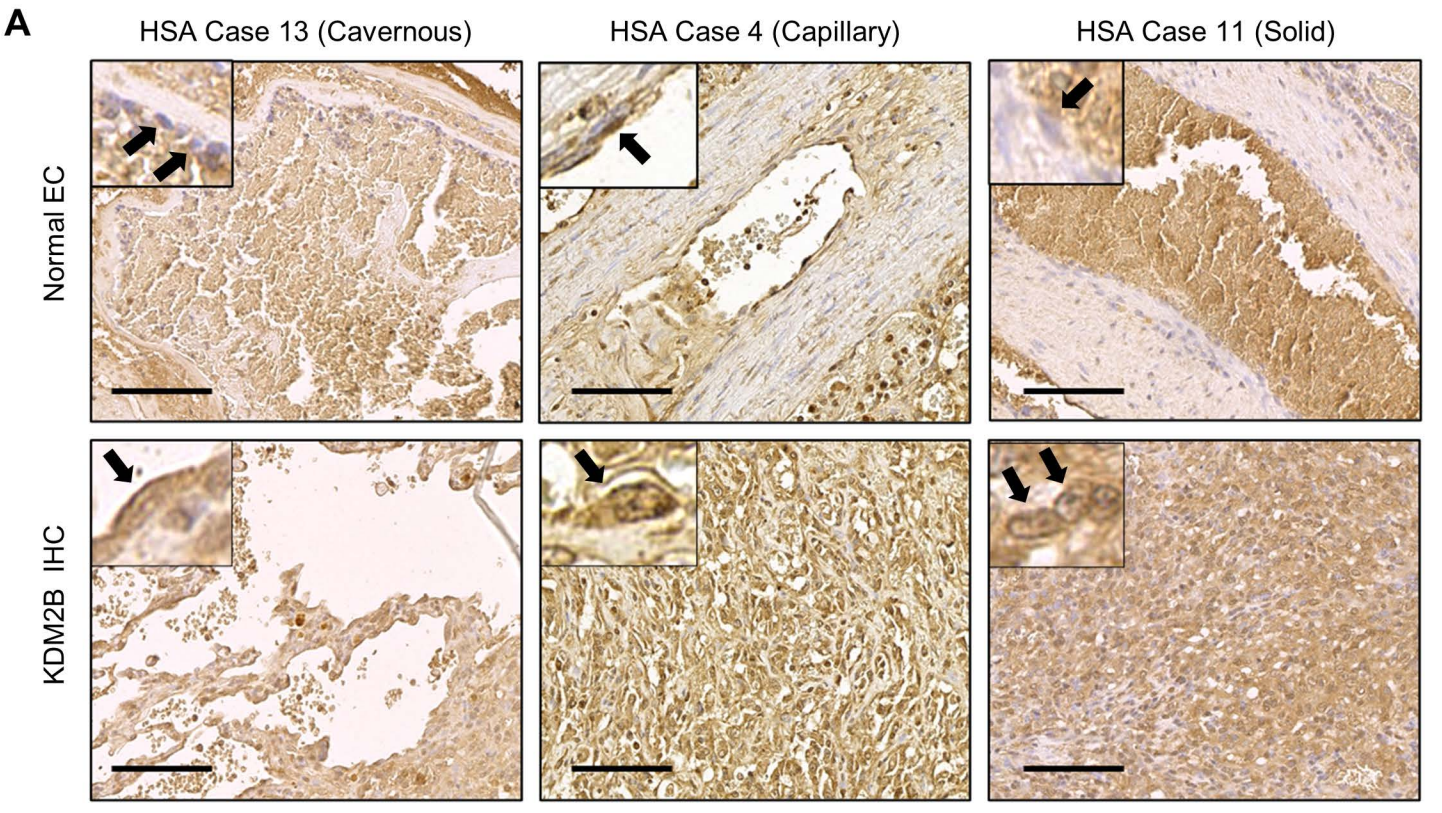
A
HSA Case 13 (Cavernous)
HSA Case 4 (Capillary)
HSA Case 11 (Solid)
Normal EC
KDM2B IHC

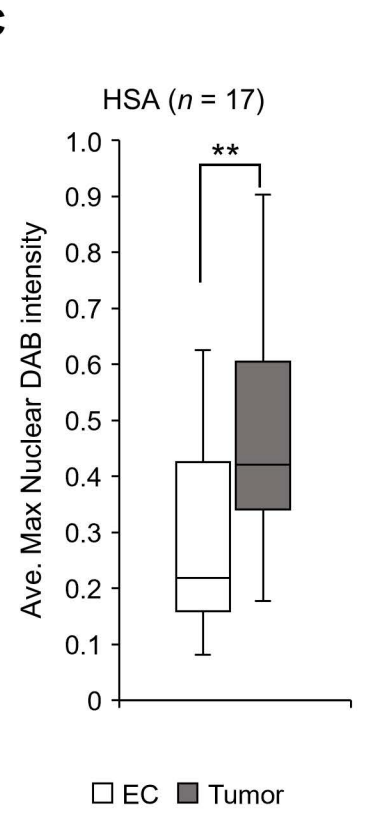
C
HSA (n = 17)
**
Ave. Max Nuclear DAB intensity
1.0
0.9
0.8
0.7
0.6
0.5
0.4
0.3
0.2
0.1
0
EC
Tumor

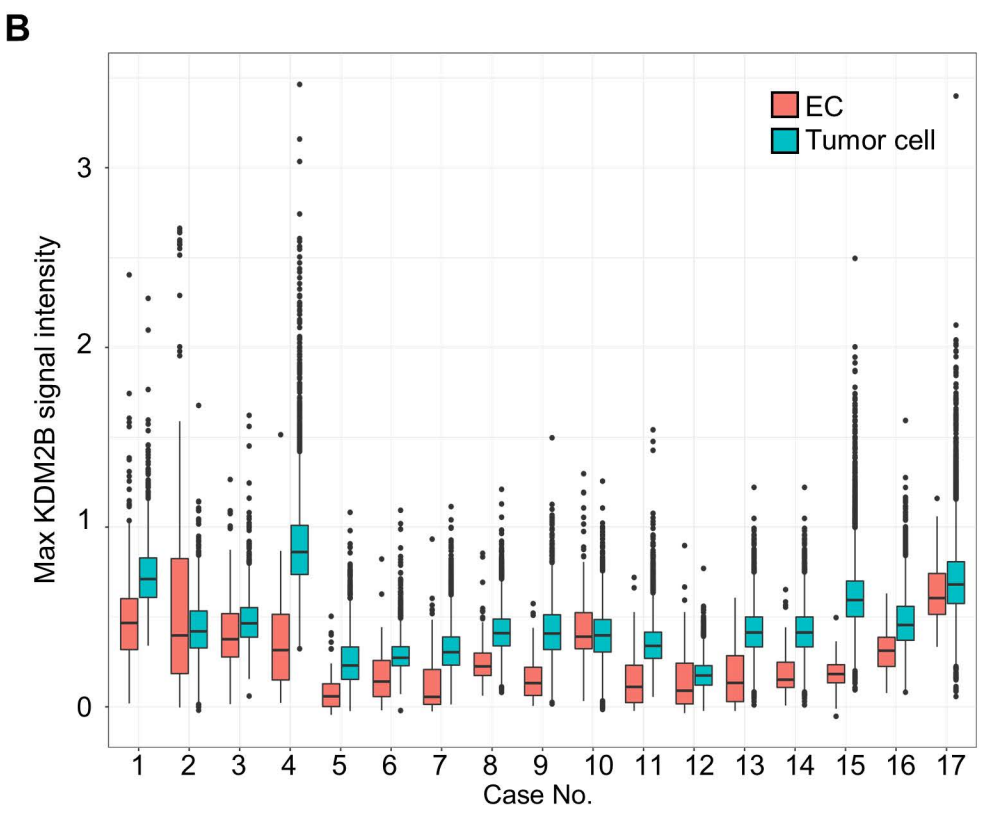
B
EC
Tumor cell
Max KDM2B signal intensity
3
2
1
0
1 2 3 4 5 6 7 8 9 10 11 12 13 14 15 16 17
Case No.

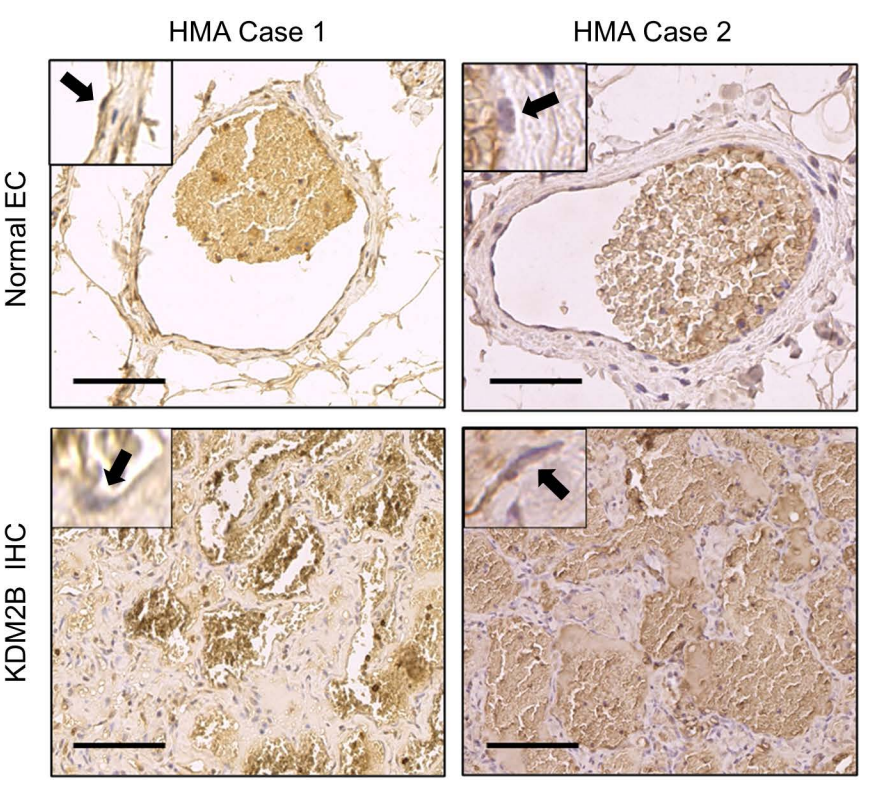
D
HMA Case 1
HMA Case 2
Normal EC
KDM2B IHC

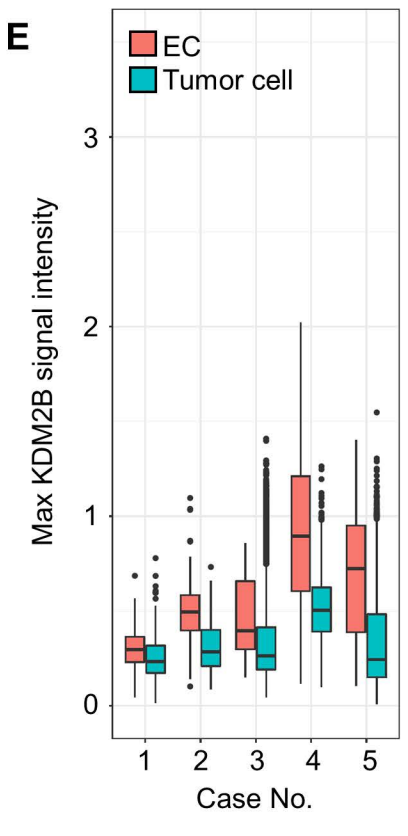
E
EC
Tumor cell
Max KDM2B signal intensity
3
2
1
0
1 2 3 4 5
Case No.

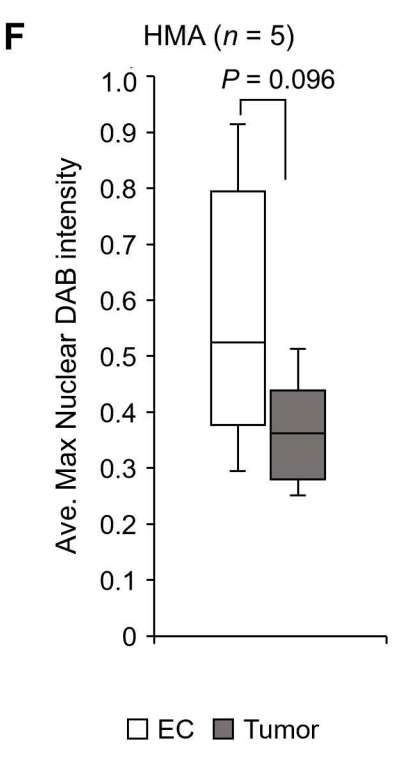
F
HMA (n = 5)
P = 0.096
Ave. Max Nuclear DAB intensity
1.0
0.9
0.8
0.7
0.6
0.5
0.4
0.3
0.2
0.1
0
EC
Tumor

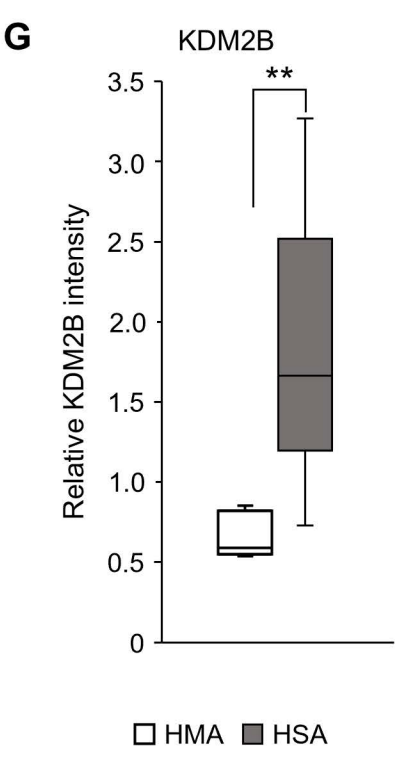
G
KDM2B
**
Relative KDM2B intensity
3.5
3.0
2.5
2.0
1.5
1.0
0.5
0
HMA
HSA

Fig. 5

A

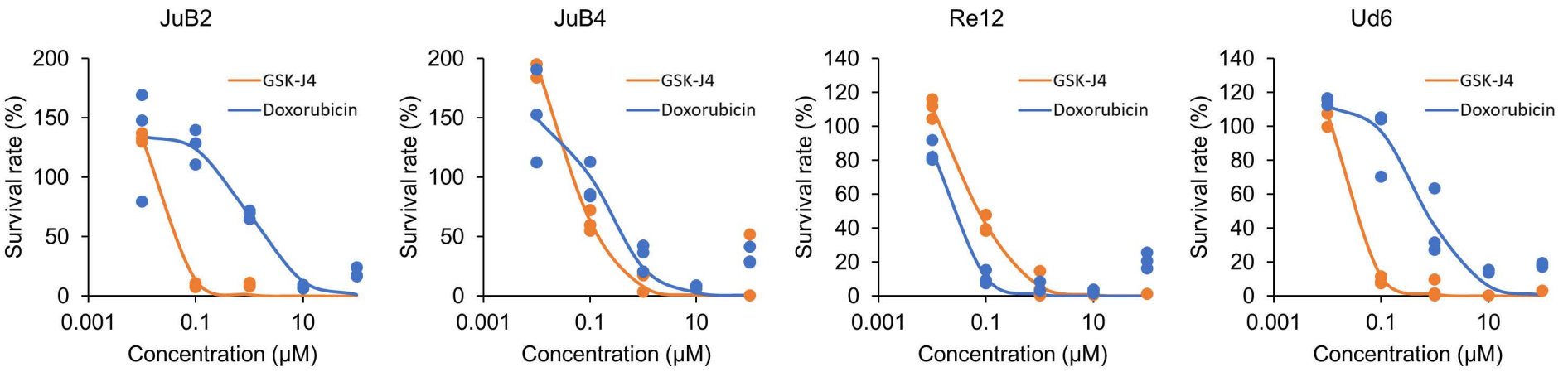

IC_{50} GSK-J4	26.8 nM
IC_{50} Doxorubicin	1.76 μM

IC_{50} GSK-J4	136 nM
IC_{50} Doxorubicin	380 nM

IC_{50} GSK-J4	77 nM
IC_{50} Doxorubicin	19.4 nM

IC_{50} GSK-J4	22.3 nM
IC_{50} Doxorubicin	727 nM

B

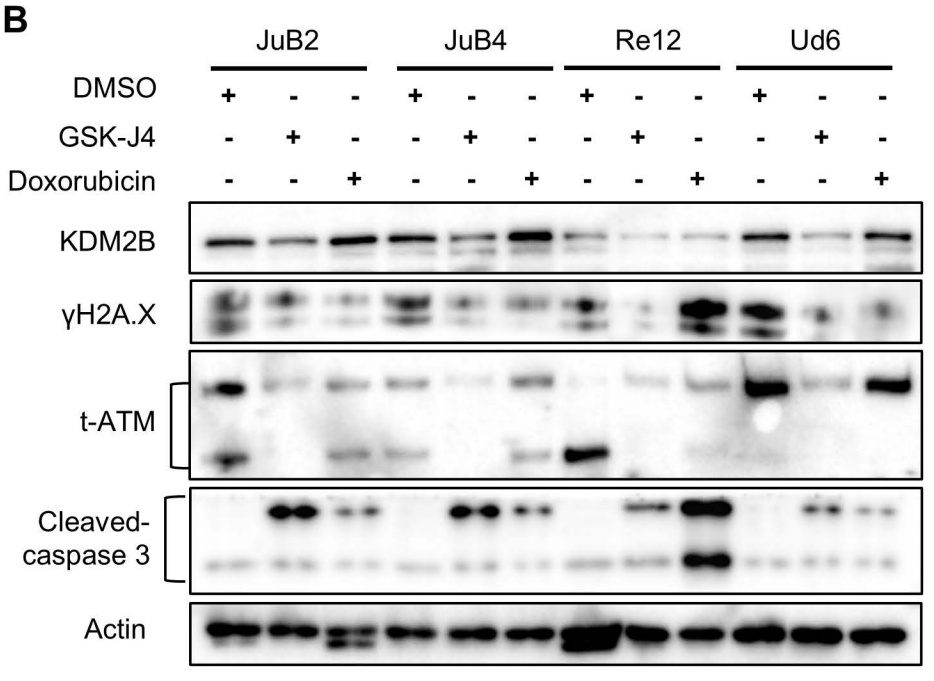

C

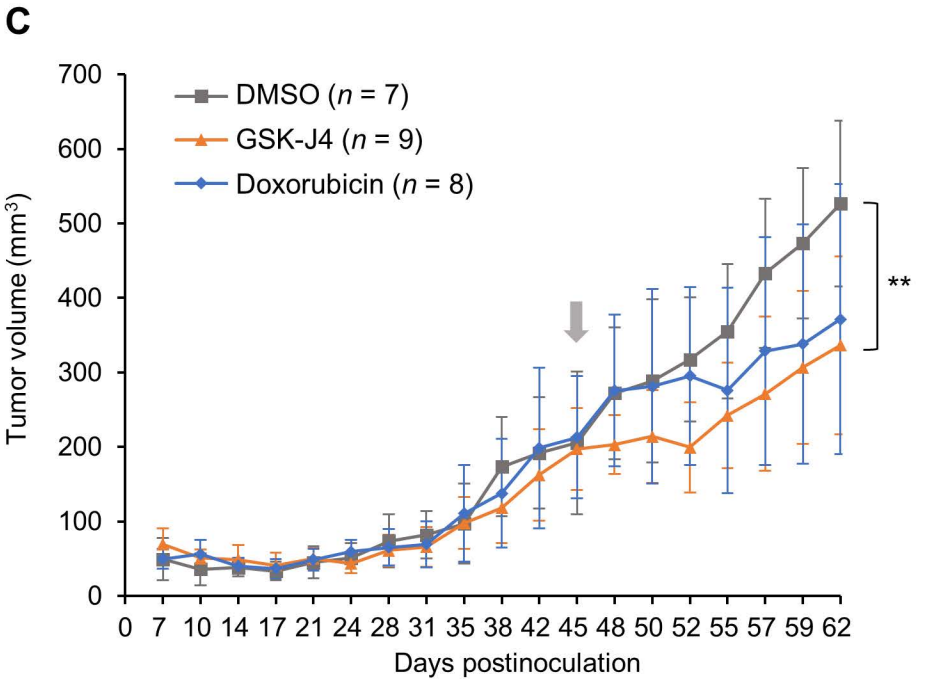

D

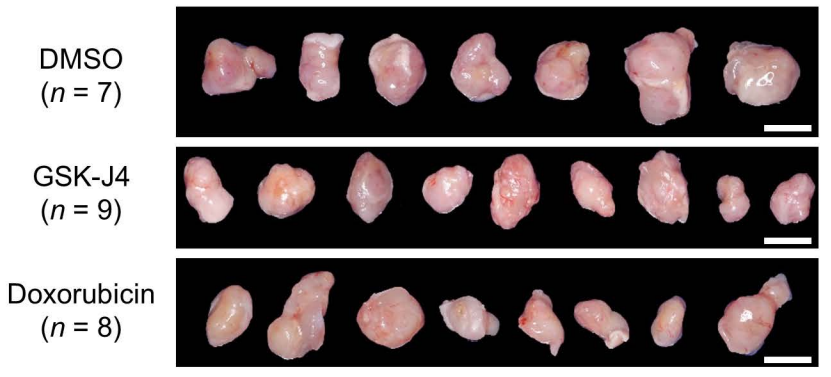

E

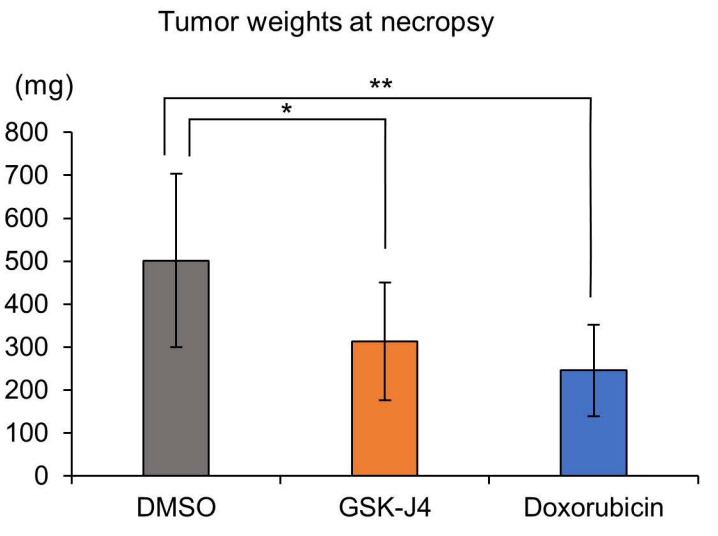

F

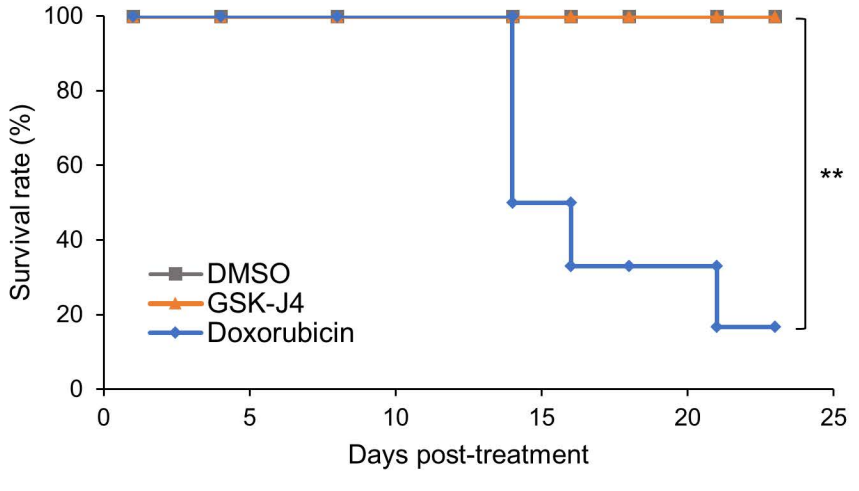

G

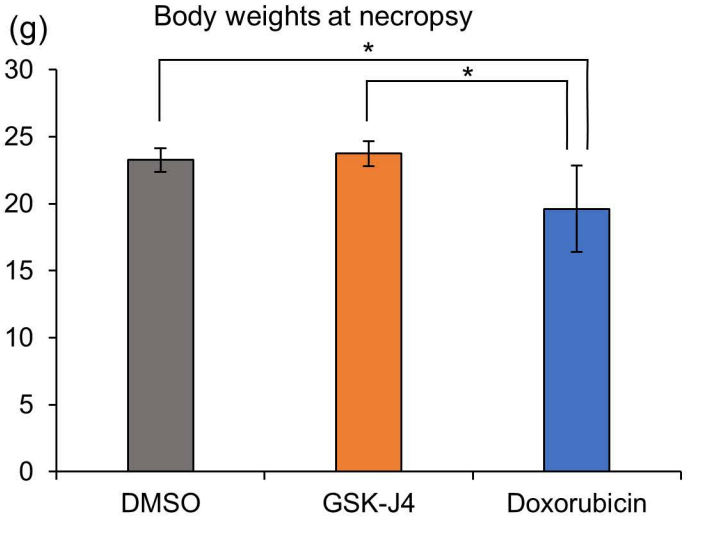

Fig. 6